J. Fluid Mech. (2024), *vol*. 996, A12, doi:10.1017/jfm.2024.762

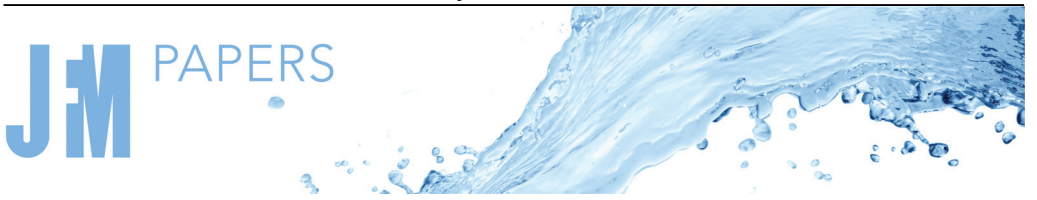

Dynamics of turbulent energy and dissipation in channel flow

Le Yin[1],†, **Yongyun Hwang**[2] **and John Christos Vassilicos**[1]

[1]UMR 9014 – LMFL – Laboratoire de Mécanique des Fluides de Lille – Kampé de Fériet, Univ. Lille, CNRS, ONERA, Arts et Metiers Institute of Technology, Centrale Lille, F-59000 Lille, France

[2]Department of Aeronautics, Imperial College London, South Kensington, London SW7 2AZ, UK

(Received 7 February 2024; revised 26 June 2024; accepted 12 August 2024)

The dynamics of turbulent kinetic energy (TKE), turbulence dissipation rate (TDR) and turbulence production rate (TPR) are explored in fully developed turbulent channel flow using direct numerical simulations up to $Re_\tau \approx 2000$ with minimal computational box for large-scale structures. Time correlation analysis based on volume-averaged TKE and TDR shows a well-defined average time lag, as in periodic/homogeneous turbulence, which, unlike periodic/homogeneous turbulence, appears to be Reynolds-number-dependent. On the basis of a spatio-temporal correlation analysis, we show that plane-averaged TKE fluctuations in the near-equilibrium region are transported towards both the core and near-wall regions, and are positively correlated with plane-averaged TDR fluctuations there with combined wall-distance and time lags. In the path towards the core region, the wall-distance lag is very close to the time lag multiplied by the friction velocity. The path towards the near-wall region has a wide spread of time lags, which increases with Reynolds number. The spatio-temporal correlation paths both towards the core and towards the wall are reproduced when the reference plane TKE is conditionally averaged on either ejections or sweeps, and are in fact stronger in correlation values in the case of ejections, which are better organised than sweeps. While volume-averaged TPR evidently precedes volume-averaged TKE, a more complex picture of non-local space–time correlations between reference plane TKE and TPR is revealed. A mechanistic model is proposed to elucidate these correlations between TKE and TPR through the interaction between the mean shear and the Reynolds shear stress.

Key words: turbulence theory, channel flow

1. Introduction

Dissipation plays an important role in the dynamics of turbulent flows. In a turbulence that is statistically stationary and homogeneous, the Richardson–Kolmogorov energy cascade

† Email address for correspondence: le.yin@centralelille.fr

states that the turbulent kinetic energy (TKE) produced at the large scales is on average carried to smaller scales and eventually dissipated at the smallest scales (Frisch 1995). An equilibrium between the space–time average rate of turbulence generation at the large scales and the space–time average turbulence dissipation at the smallest scales is achieved. However, highly active fluctuations in TKE and turbulence dissipation rate (TDR) appear if such averaging is removed. The feeding and dissipation of turbulence are almost always out of equilibrium. For example, the studies of Goto & Vassilicos (2015, 2016) in forced periodic/homogeneous turbulence showed that the volume-averaged TDR $\varepsilon_V(t)$ fluctuates in time and correlates heavily with the volume-averaged TKE $E_V(t)$ with some finite time lag that characterises the average time taken for the turbulence cascade to transport energy from the large energy-containing scales to the small dissipative scales (see Sagaut & Cambon 2008). They also demonstrated that the turbulence dissipation coefficient, defined as $C_\varepsilon(t) \equiv \varepsilon_V/(E_V^{3/2}/L)$ (where $L = L(t)$ is the fluctuating integral length scale), is anti-correlated in time with the Taylor-length-based Reynolds number $Re_\lambda(t) \sim E_V/\sqrt{\nu\varepsilon_V}$ (where ν is the kinematic viscosity) without time lag, i.e. $C_\varepsilon(t) \sim (\sqrt{Re_G}/Re_\lambda(t))^n$, where $n \approx 1$ and Re_G denotes a global Reynolds number. Here, C_ε is a ratio between the rate of energy loss (dissipation) at the small scales and the rate of energy loss at the large scales (by the large-scale eddy turnover). Similarly, Re_λ is a ratio of the energy E_V contained mainly in the large scales to the energy $\sqrt{\nu\varepsilon_V}$ contained in the small scales. The strong anti-correlation between C_ε and Re_λ suggests that the turbulence is self-regulating: when the energy at the large scales becomes excessive compared to the energy at the small scales, the large scales tend to lose energy at a higher rate compared to the rate of energy loss at the small scales. This self-regulation appears to be a universal phenomenon that is present, in one way or another, in a wide range of turbulent flows (see Vassilicos 2015; Vassilicos & Laval 2024).

Recently, Apostolidis, Laval & Vassilicos (2022) investigated this self-regulation (using wall-parallel plane average quantities instead of volume-averaged ones) in the near-equilibrium region of fully developed turbulent channel flow (FD TCF), where the local turbulence energy production roughly balances local turbulence energy dissipation on average (Townsend 1961), and found an exponent $n \approx 3/2$ for the time fluctuations. It was even further demonstrated that the two signals are anti-correlated at all frequencies in this region of FD TCF. However, they did not investigate the possibility of a time lag between TKE and TDR in FD TCF.

The key difference between wall-bounded turbulence and periodic/homogeneous turbulence is the coupling between the boundary conditions and the generation of turbulence. In periodic/homogeneous turbulence, TKE is generated by arbitrary direct forcing of the Navier–Stokes equations, whereas in TCF, the no-slip boundary condition at the wall enforces mean shear and momentum transfer between the core flow and the wall, thereby leading to production of TKE. Both viscosity and turbulence (through the Reynolds shear stress, which is an average of $u'v'$, where u' and v' are streamwise and wall-normal velocity fluctuations, respectively) contribute to the momentum transfer, and the latter is particularly significant away from the wall where the effect of viscosity is negligible. The contributions of Reynolds shear stress can be classified based on the sign of velocity fluctuations, i.e. the quadrant in u'–v' plane (Wallace, Eckelmann & Brodkey 1972; Willmarth & Lu 1972; Lu & Willmarth 1973). In particular, ejections (Q2 quadrant, where $u' < 0$ and $v' > 0$) provide the largest contribution to the Reynolds stress, and sweeps (Q4 quadrant, where $u' > 0$ and $v' < 0$) provide the second largest contribution to the Reynolds stress throughout a turbulent boundary layer (Lu & Willmarth 1973).

Thanks to the development of numerical simulation and high performance computing, spatio-temporal data of turbulence fields have been made available. In the numerical experiment of Jiménez & Moin (1991), the width of the minimal computational domain (minimal flow unit) that can sustain TCF was found to be approximately the average spacing of near-wall streaks discovered from the early experiment of Kline *et al.* (1967). By removing the small-scale structures using over-damped large eddy simulation, Hwang & Cossu (2010) identified the largest energy-containing structures in the outer layer that conform with the large- and very-large-scale motions (Kim & Adrian 1999; Guala, Hommema & Adrian 2006; Hutchins & Marusic 2007*a*).

Energy-containing structures regenerate themselves quasi-periodically, and constitute a substantial part of the dynamics of wall-bounded flows (Hamilton, Kim & Waleffe 1995; Waleffe 1997; Jiménez & Pinelli 1999; Hwang & Bengana 2016). This autonomous cycle is often referred to as the 'self-sustaining process' (Doohan, Willis & Hwang 2021; Ciola *et al.* 2023). Recent studies on the time evolution of these energy-containing structures suggest that they operate quasi-periodically with a time scale proportional to their size (Lozano-Durán & Jiménez 2014*b*; Hwang & Bengana 2016).

In the present study, we explore the dynamical interplay between TKE, TDR and turbulence production rate (TPR) fluctuations in a relatively small computational box FD TCF at moderately high Reynolds number. Whereas there was no need to study the fluctuations of power input rate in the studies of periodic/homogeneous turbulence of Goto & Vassilicos (2015, 2016), which concentrated on TKE and TDR fluctuations, in FD TCF the TPR fluctuations are part and parcel of small box dynamics and cannot be neglected. We start by exploring the same questions addressed by Goto & Vassilicos (2015, 2016), but now in FD TCF, namely whether TKE and TDR fluctuate in a quasi-periodic manner, and whether they do so with some time lag relative to each other as in forced periodic/homogeneous turbulence. If so, what are the scalings of this time lag, and does it relate to the dynamics of TPR in wall-bounded flows? We finally address the interconnectivity between TPR and TKE dynamics given that TKE needs to be produced before it is cascaded to smaller scales and dissipated.

While such general questions can be asked for any wall-bounded turbulent flow, we limit ourselves to the study of FD TCF using direct numerical simulations (DNS) datasets at several different Reynolds numbers with long integration time intervals to obtain well-converged statistics and temporal correlations. The size of the computational box is chosen to be the minimal one that can accommodate the largest energy-containing structures in FD TCF as in Hwang & Cossu (2010) without mean statistics, such as time-averaged mean velocity profile and mean energy budgets deviating too far from DNS in larger computational domains (Lozano-Durán & Jiménez 2014*a*; Lee & Moser 2015).

This paper is organised as follows. In § 2, we present the numerical set-up for our DNS of FD TCF, and define our observables in terms of turbulence energetics. In § 3, we present our results on the dynamics of TKE and TDR in terms of volume-averaged temporal correlations, 2-time 1-plane correlations, and 2-time 2-plane correlations of plane-averaged turbulence energetics. We then focus in § 4 on TPR and TKE fluctuations, as well as fluctuations of Reynolds shear stress and mean shear, and introduce a mechanistic model of the fluctuations of mean shear and Reynolds shear stress to account for the space–time lags between TPR and TKE. We summarise our conclusions in § 5.

2. Numerical methods

We perform DNS of incompressible FD TCF subject to constant mass flux at five different Reynolds numbers $Re_\tau = 235, 359, 498, 953, 2008$, where Re_τ is the friction Reynolds

Name	Re_τ	$N_x \times N_y \times N_z$	Δx^+	Δy^+	Δz^+	$T_{int} u_\tau / H$	N_t
R230	235	$96 \times 193 \times 96$	11.52	0.53–4.53	5.76	183.06	3000
R360	359	$144 \times 257 \times 144$	11.74	0.61–5.19	5.87	172.13	3000
R500	498	$192 \times 289 \times 192$	12.22	0.75–6.41	6.11	164.34	3000
R950	953	$384 \times 513 \times 384$	11.69	0.80–6.91	5.85	151.52	3000
R2000	2008	$768 \times 1025 \times 768$	12.31	0.83–7.29	6.16	92.42	2001

Table 1. Numerical set-up of DNS in FD TCF, where N_x, N_y and N_z indicate the numbers of grid points in the streamwise, wall-normal and spanwise directions, respectively; Δx^+, Δy^+ and Δz^+ indicate grid spacings, after de-aliasing, in inner units; T_{int} denotes the integration time after the initial transient; and N_t denotes the number of instantaneous snapshots stored for post-processing.

number. We denote the streamwise, wall-normal and spanwise directions by (x, y, z), with the corresponding velocity fields (u, v, w) or (u_1, u_2, u_3). The size of the simulation domain is set to be $L_x = \pi H$, $L_y = 2H$ and $L_z = \pi H/2$, where H is the half-channel height. The spanwise extent of the simulation box is comparable to the minimal unit for the self-sustaining process of the largest energy-containing structures as per Hwang & Cossu (2010) and Hwang & Bengana (2016). The size of the simulation domain is deliberately chosen to be small in order to capture the temporal dynamics around the single entity of the large-scale energy-containing structures without significantly modifying the mean statistics (Lozano-Durán & Jiménez 2014*a*). Details of the DNS data sets and their naming convention can be found in table 1. We note that integration over a relatively long time interval is required to obtain well-converged statistics 'temporal correlations' in the given computational domain.

The numerical simulation is performed using the Navier–Stokes solver diablo (Bewley 2014). The solver uses the Fourier–Galerkin method with a 2/3 de-aliasing rule in the wall-parallel directions x and z, and a second-order finite difference method in the wall-normal direction y. The temporal discretisation of the solver is based on the fractional-step algorithm by Kim & Moin (1985), with implicit treatment of viscous terms using the Crank–Nicolson scheme, and explicit treatment of the remaining terms using a low-storage third-order Runge–Kutta scheme. A snapshot of the velocity field is stored every $1H/U_b$, where $U_b = (1/V_\Omega) \int_\Omega u \, \mathrm{d}^3\boldsymbol{x} = 1$ (with Ω the computational domain, and V_Ω its volume) is the bulk streamwise velocity that is kept constant at all time in all DNS. The solver has been verified extensively in previous studies (e.g. Doohan, Willis & Hwang 2019).

3. Dynamics of TKE and TDR

We first study the dynamics of the TDR and its relation to TKE from the temporal correlation of terms in the TKE budget equation in the wall-normal direction and in time. The velocity field is decomposed as $\boldsymbol{u}(\boldsymbol{x}, t) = (U(y, t), 0, W(y, t)) + \boldsymbol{u}'(\boldsymbol{x}, t)$, where $(U(y, t), 0, W(y, t)) = \langle \boldsymbol{u}(\boldsymbol{x}, t) \rangle$, and $\langle \cdot \rangle$ denotes averaging over the x–z plane. While the Reynolds decomposition has often been used with a mean flow obtained by averaging over time, here we average over wall-parallel planes and extract a time-fluctuating average flow profile, from which the associated Reynolds stresses are derived. Both the average flow and the Reynolds stresses fluctuate in time because of the finite size of the minimal computational domain. We use the notation $\boldsymbol{x} \equiv (x_1, x_2, x_3) \equiv (x, y, z)$ and $(u'_1, u'_2, u'_3) \equiv (u', v', w')$, and two energy budget equations can be considered. The first is for the kinetic

energy $(U^2 + W^2)/2$ of the mean flow, which involves neither turbulence transport nor small-scale turbulence dissipation (the dissipation rate in this equation is $\nu[(\mathrm{d}U/\mathrm{d}y)^2 + (\mathrm{d}W/\mathrm{d}y)^2]$, which, unlike TDR, cannot result from a turbulence cascade in (x, y, z) space). The second equation is for the TKE, $\langle u_i' u_i' \rangle/2$, which does incorporate turbulence transport and cascade-related dissipation dynamics, and is obtained by multiplying the governing equation for the fluctuating velocity component u_i' by u_i', summing over $i = 1, 2, 3$ and averaging in the x–z plane:

$$\underbrace{\frac{\partial}{\partial t}\frac{1}{2}\langle u_i' u_i' \rangle}_{E(y,t)} = \underbrace{-\left\langle u_i' u_j' \right\rangle \frac{\partial U_i}{\partial x_j}}_{P(y,t)} \underbrace{-\nu \left\langle \frac{\partial u_i'}{\partial x_j}\frac{\partial u_i'}{\partial x_j} \right\rangle}_{\varepsilon(y,t)} + \underbrace{\frac{\mathrm{d}}{\mathrm{d}y}\langle -v'(u_i' u_i') \rangle}_{T_t(y,t)} + \underbrace{\nu \frac{\mathrm{d}^2}{\mathrm{d}y^2}\frac{1}{2}\langle u_i' u_i' \rangle}_{T_\nu(y,t)} + \underbrace{\frac{\mathrm{d}}{\mathrm{d}y}\langle -v'p' \rangle}_{T_p(y,t)}, \tag{3.1}$$

where ν is the kinematic viscosity of the fluid, $p' \equiv p - \langle p \rangle$ is the fluctuating pressure field, and p is the full pressure field (the mass density of the fluid is taken to be 1). Note that the three transport terms given in the second line of (3.1) vanish when integrating throughout the wall-normal direction because of the no-slip boundary condition at the walls. This is not true if we integrate only over the half-channel in the wall-normal direction from the wall to the channel centre, where the fluxes are expected to be highly fluctuating in time.

In this paper, we focus on the TKE budget (3.1) because this is the budget directly affected by turbulence cascade (via TDR) and turbulence transport. A top-down approach is employed to study the correlations in FD TCF between TKE $E(y, t)$ and TDR $\varepsilon(y, t)$ on the one hand, and TPR $P(y, t)$ and TDR $\varepsilon(y, t)$ on the other. We first explore the dynamics of the overall TKE and TDR by studying the temporal correlation between their volume averages in § 3.1, as in the work of Goto & Vassilicos (2015) for periodic/homogeneous turbulence. We volume average from either wall to the centreline, and report the existence of a time lag both between volume-averaged TKE and volume-averaged TDR, and between volume-averaged TPR and volume-averaged TDR. (For all present Reynolds numbers, the frequency spectrum of the volume average $U^2/2$ has 1–2 orders of magnitude more energy density than the volume-averaged TKE frequency spectrum at frequencies below $0.5H/u_\tau$ to H/u_τ. The two frequency spectra are, however, comparable at higher frequencies, and the intensity of time fluctuations of the volume-averaged $U^2/2$ is approximately 1 % of its time average, whereas the intensity of time fluctuations of the volume-averaged TKE is about 10 % of its time average. Here, $W^2/2$ is very much smaller than TKE with negligible fluctuations.) More detailed dynamical interplay between TKE and TDR is subsequently studied in the wall-normal direction by investigating in § 3.2 the temporal correlation of the plane-averaged TKE and the plane-averaged TDR at the same wall-normal location. Overall, the temporal correlation between the two signals is high in the near-wall and outer regions, but little time lag is observed, suggesting that the time lag observed from the volume-averaged statistics results from dynamics involving various wall-normal locations. In § 3.3, we therefore investigate the temporal correlation between plane-averaged TKE and plane-averaged TDR at different wall-normal locations, i.e. $\varepsilon(y, t)$ and $E(y^{ref}, t)$, where y^{ref} is a reference wall-normal location. A time lag between TKE and TDR is recovered together with a wall-distance lag, revealing the role of inhomogeneity in the spatio-temporal path of energy transfer in FD TCF which is absent

in the temporal correlation between plane-averaged TPR and plane-averaged TDR. We also report significant temporal anti-correlations in the near-equilibrium region between TKE and TDR with time lag. In § 3.4, we investigate the 2-time 2-plane correlations with reference plane taken in the near-wall region, and report a Reynolds number dependence of correlation contours. We then average TKE and TDR over regions of ejection and sweeps to further illustrate the link between paths of energy and momentum fluxes in FD TCF in § 3.5.

3.1. *Volume-averaged dynamics and correlations*

The volume-averaged budget equation is obtained by integrating (3.1) from either wall to the centre of the channel:

$$\frac{\partial}{\partial t}E_V = P_V - \varepsilon_V \pm T|_{y=H}, \tag{3.2}$$

where the subscript V denotes averaging over the upper or lower half of the computational domain. Without time averaging, the wall-normal transport terms in (3.1) fluctuate in time. The fluxes $\pm T|_{y=H}$ across the centreline are found to be very small compared with the integrated turbulence production P_V and dissipation ε_V.

Figures 1(*a*,*d*,*g*,*j*,*m*) present the time signals of volume-averaged TPR, TKE and TDR for R230, R360, R500, R950 and R2000 (see table 1). While these signals fluctuate heavily around their mean values, TDR seems to have a low frequency content that closely follows TPR and TKE, together with some coexisting high-frequency content, a behaviour that becomes more apparent with increasing Reynolds number. The time signal of TDR in FD TCF more explicitly displays various time scales other than that of TKE, particularly at higher Reynolds numbers, unlike previous observations in homogeneous turbulence (Goto & Vassilicos 2015). This difference might be attributed to the presence of a hierarchy of energy-containing scales or integral length scales in FD TCF.

The time histories of volume-averaged TKE and volume-averaged TDR in (3.2) are subsequently studied using a temporal correlation function. For two random signals that fluctuate only in time, say $X(t)$ and $Y(t)$, the temporal correlation function is defined as

$$\rho_{[X,Y]}(\tau) = \frac{\overline{X'(t+\tau)\,Y'(t)}}{\sqrt{\overline{X'^2(t)}}\sqrt{\overline{Y'^2(t)}}}, \tag{3.3}$$

where $X'(t) = X(t) - \bar{X}$ is the fluctuation centred around its mean, and $\bar{X}$ is the time average of $X(t)$. The auto-correlation function is recovered for $X(t) = Y(t)$, in which case a maximum value $\rho_{[X,X]}(\tau) = 1$ is reached for time lag $\tau = 0$.

The temporal correlation functions are presented in figures 1(*b*,*c*,*e*,*f*,*h*,*i*,*k*,*l*,*n*,*o*). Limited by the Reynolds number, R230 and R360 show narrow auto-correlation of volume-averaged TKE. The auto-correlation functions of volume-averaged TKE cross zero at $\tau u_\tau/H \approx \pm 2$ for the higher three Reynolds numbers shown here, suggesting that some aspects, at least, of the dynamics and time scales of large-scale energy-containing structures become approximately independent of Reynolds number when it is high enough (Hwang & Bengana 2016). The auto-correlation functions in figures 1(*b*,*e*,*h*,*k*,*n*) show sharper correlation peaks for TDR and TPR than for TKE, presumably caused by the high-frequency content in the dissipation and production signals. The zero crossings of the auto-correlation for TDR and TPR widen as the Reynolds number increases, although it remains unclear if this continues with further increasing Reynolds number. Importantly, the peaks of the correlation functions between volume-averaged TKE and

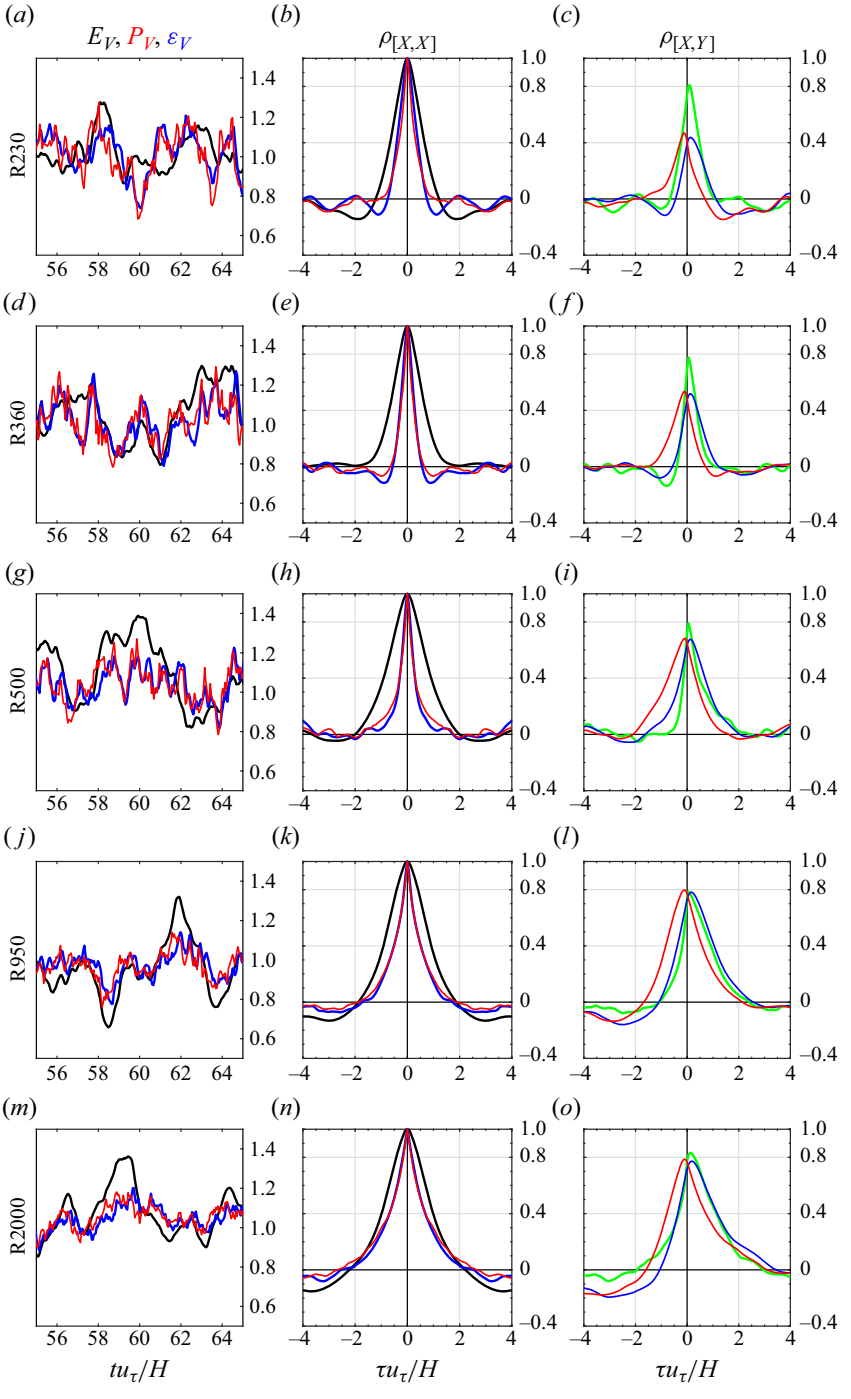

Figure 1. (*a*,*d*,*g*,*j*,*m*) Time evolution of volume-averaged TKE $E_V(t)$ (black lines), volume-averaged TDR $\varepsilon_V(t)$ (blue lines) and volume-averaged TPR $P_V(t)$ (red lines), normalised by their time-averaged mean in the lower half-channelfor five Reynolds numbers. (*b*,*e*,*h*,*k*,*n*) Auto-correlations $\rho_{[E_V,E_V]}$ (black lines), $\rho_{[\varepsilon_V,\varepsilon_V]}$ (blue lines) and $\rho_{[P_V,P_V]}$ (red lines). (*c*,*f*,*i*,*l*,*o*) Cross-correlations $\rho_{[\varepsilon_V,E_V]}$ (blue lines), $\rho_{[P_V,E_V]}$ (red lines) and $\rho_{[\varepsilon_V,P_V]}$ (green lines).

volume-averaged TDR are at $\tau u_\tau/H \approx 0.2$, with values of $\rho_{[\varepsilon_V,E_V]}$ between 0.5 and 0.8 (increasing with Re_τ), indicating the presence of an average time lag that is reminiscent of the observations made in forced periodic/homogeneous turbulence by Goto & Vassilicos (2015) (see also figure 3(*b*) in Goto & Vassilicos 2016). A similar time lag is also observed between volume-averaged TPR and volume-averaged TDR, in fact with even higher values $\rho_{[\varepsilon_V,P_V]}$ (consistently approximately 0.8 for all five Reynolds numbers) presumably because TPR and TDR are both rates of change of TKE. This time lag is shorter than the typical time scale of the self-sustaining process at large scale (Hwang & Bengana 2016). In addition, the correlation functions $\rho_{[\varepsilon_V,E_V]}$ and $\rho_{[\varepsilon_V,P_V]}$ display increasing skewness towards positive time lags at higher Reynolds numbers, spanning the range $\tau u_\tau/H \in [-1, 2]$ for R550 but $\tau u_\tau/H \in [-1, 4]$ for R2000 in the case $\rho_{[\varepsilon_V,E_V]}$. The skewed correlation function may be interpreted as a 'spread' of time lags (see § 3.3).

While we observe a clear positive time lag both between TKE and TDR and between TPR and TDR in FD TCF, it is important to point out that volume averaging obscures the dynamics associated with inhomogeneity in the interactions between TKE and dissipation. The observed dynamical interplay between TKE and TDR cannot be the same as that found in periodic/homogeneous turbulence (Goto & Vassilicos 2015). We address the impact of vertical inhomogeneity on the interplay between TKE and TDR in the remainder of § 3, and the interplay between TKE and TPR in § 4.

3.2. *The 2-time 1-plane correlations*

The neglect of inhomogeneity, due to volume averaging, needs to be restored for the detailed picture of the full temporal dynamics between TKE and TDR. We therefore now investigate, as in § 3.1, the correlations between time signals of plane-averaged TKE and plane-averaged TDR at different wall-normal locations. In figure 2, we plot time signals of the plane-averaged TKE and TDR normalised by their plane- and time-averaged mean values at three locations: the near-wall region at the edge of the viscous sublayer ($y^+ = 10$), the near-equilibrium region where production approximately balances dissipation ($y/H = 0.3$), and the core region ($y/H = 0.8$).

In the near-wall region ($y^+ = 10$ in figure 2, but similar observations hold for $y^+ \leqslant 100$), TKE and turbulence dissipation fluctuate almost concurrently. This is not surprising as there is little separation between the energy-containing scale and dissipative scale in the near-wall region. As the Reynolds number increases (from top to bottom in figure 2), the low frequency signal appears more pronounced. The near-wall time scale becomes shorter and shorter compared to H/u_τ (used to normalise time in figure 2) as Reynolds number increases. It is interesting to observe that even so, TKE and TDR fluctuate almost concurrently even at the highest Reynolds numbers considered here (see figures 2*j*,*m*). This suggests that the near-wall energy-containing structures (potentially part of large-scale structures extending from the near-equilibrium and outer layers) are directly related to dissipation in the near-wall region.

At $y/H = 0.3$ (figures 2*b*,*e*,*h*,*k*,*n*), the time signals of plane-averaged TKE and plane-averaged TDR do not appear to be well correlated with each other as Re_τ increases. The same holds true for any y/H between 0.2 and 0.4. Note that this is the region where the large-scale structures are very energetic (Hoyas & Jiménez 2006).

In the core region at $y/H = 0.8$ (though similar observations can be made for $y/H = 0.5$–1), TPR is known to be very small due to diminishing mean shear and Reynolds shear stress near the channel centre. The dynamics of turbulence energetics is

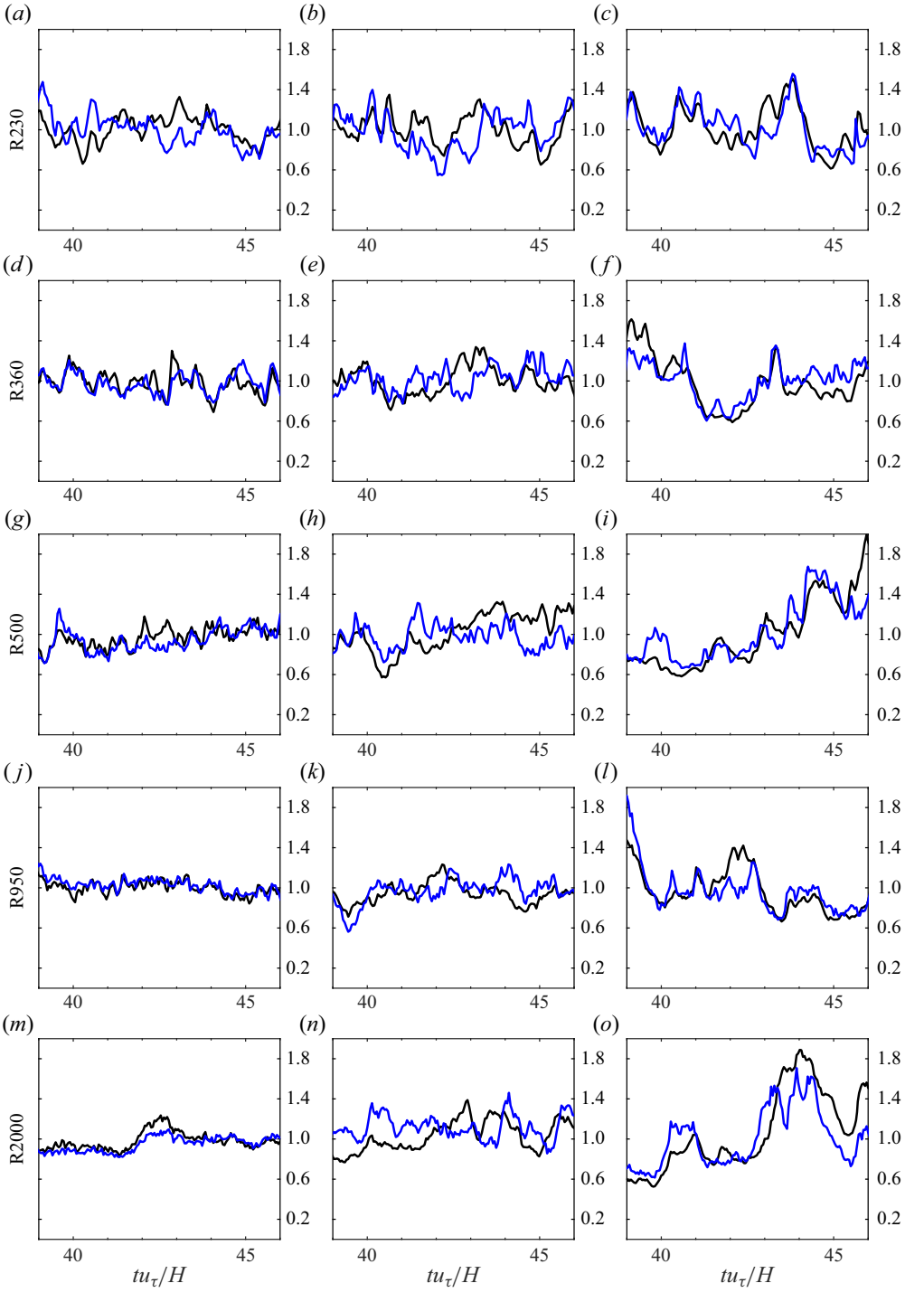

Figure 2. Time evolution of plane-averaged TKE $E(y, t)$ (black lines) and plane-averaged TDR $\varepsilon(y, t)$ (blue lines), normalised by their plane- and time-averaged mean in the lower half-channel for five Reynolds numbers at three wall-normal locations: (*a*,*d*,*g*,*j*,*m*) $y^+ = 10$, (*b*,*e*,*h*,*k*,*n*) $y/H = 0.3$, and (*c*,*f*,*i*,*l*,*o*) $y/H = 0.8$.

therefore dominated by turbulence transport and dissipation. The plane-averaged TKE and the plane-averaged TDR appear highly correlated instantaneously at the same plane, as shown in figures 2(*c*,*f*,*i*,*l*,*o*) for all the Reynolds numbers considered here. As can be seen in figure 3, there is no time lag in these correlations, and there is therefore no cascade directly linking plane-averaged TKE and plane-averaged TDR in the core region.

Similar to the correlation function defined for volume-averaged variables in time in § 3.1, one can define a temporal correlation function for signals in time that depends on the wall-normal location in FD TCF. Figure 3 plots the contours of 2-time 1-plane correlation functions between plane-averaged TKE and TDR, defined as

$$\rho_{[\varepsilon,E]}(\tau, y) = \frac{\overline{\varepsilon'(t+\tau, y)\, E'(t, y)}}{\sqrt{\overline{\varepsilon'^2(t, y)}}\sqrt{\overline{E'^2(t, y)}}}, \tag{3.4}$$

where τ is a time difference. From the correlation contours in figure 3, high positive correlations between TDR and TKE in the near-wall region and the core region with zero time lag are observed, as expected from figure 2. The positive correlations in the near-wall region are concentrated in a narrow time window for small Reynolds numbers, which widens as Reynolds number increases, reflecting the volume-averaged correlation observation in figures 1(*c*,*f*,*i*,*l*,*o*). It may be that as Re_τ increases, increasingly energetic structures above the near-wall region influence the near-wall region with fluctuations of increasing length and time scales, causing positive correlations with an increasing range of time lags in the near-wall region. In the near-equilibrium region, the correlation contour shows negative values (anti-correlation) between TDR and TKE with positive time lag, i.e. an increase/decrease in local TKE precedes a decrease/increase in local TDR. Finally, TKE and TDR are strongly correlated throughout the core with both positive and negative time lags τ in the range $\tau u_\tau/H \in [-1, 1]$ nearly independent of Reynolds number.

In both the near-wall and core regions, the location of the maximum correlation in terms of time lag is always clearly at $\tau = 0$. In the near-equilibrium region, it is also near $\tau = 0$, though less rigorously at $\tau = 0$ because of low correlation values there. These zero time lag results have been reported previously for FD TCF (see figure 5(*g*,*h*) of Apostolidis *et al.* 2022) using data obtained in a computational domain that is double the size of the present simulations in the streamwise and spanwise directions in terms of multiples of H (Lozano-Durán & Jiménez 2014*a*). In the near-wall region, high instantaneous correlations between TKE and TDR (neither time lag nor lead) are expected, since there is no scale separation there. The high instantaneous correlations in the core region (neither time lag nor lead) suggest that high/low values of TKE and TDR occur together perhaps because the core flow flip-flops between quiescent and turbulent states as shown in Kwon *et al.* (2014). However, the zero average time lag of plane-averaged dynamics is seemingly inconsistent with the time lag discovered in volume-averaged dynamics in § 3.1. It is therefore natural to question if plane-averaged TKE at some distance from the wall correlates with plane-averaged TDR at another distance from the wall, with or without time lag.

3.3. *The 2-time 2-plane correlations: TKE and TDR*

To unveil the time lag observed in figure 1 and to illuminate the dynamic relation between TKE and TDR (as well as TPR and TDR) in space and time, we now investigate 2-time 2-plane correlations. The correlations between TKE at a reference x–z plane and TDR at

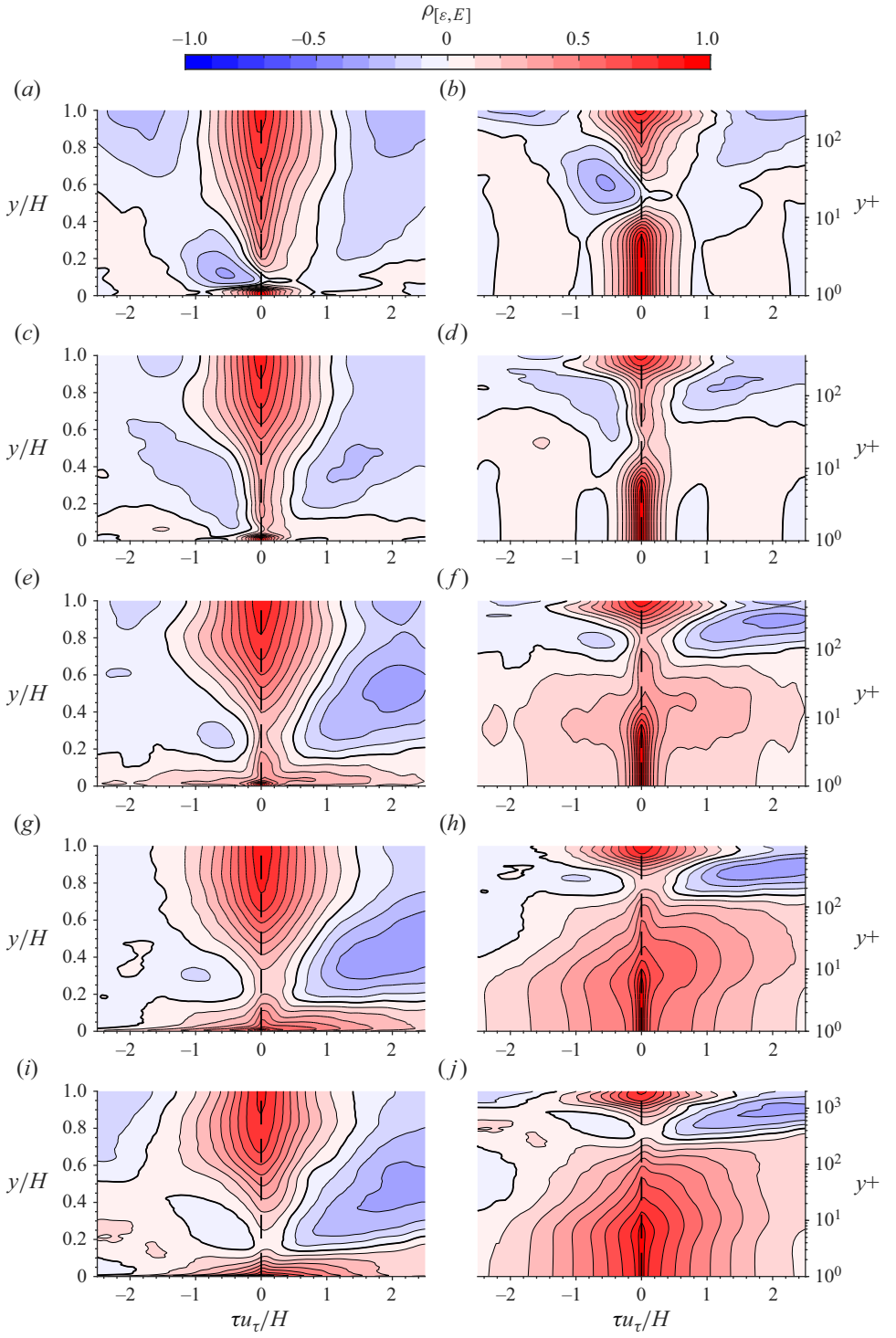

Figure 3. The 2-time 1-plane correlation function contours $\rho_{[\varepsilon,E]}$ versus distance from the wall in (*a*,*c*,*e*,*g*,*i*) outer unit y/H with linear axis, or (*b*,*d*,*f*,*h*,*j*) inner unit y^+ with log axis, and versus time lag $\tau u_\tau/H$, for (*a*,*b*) R230, (*c*,*d*) R360, (*e*,*f*) R500, (*g*,*h*) R950, (*i*,*j*) R2000. Vertical dashed lines indicate the position of maximum positive correlation as a function of y, showing that it coincides with the vertical $\tau = 0$ line.

another plane in the channel are defined as

$$\rho_{[\varepsilon,E^{ref}]}(\tau, y; y^{ref}) = \frac{\overline{\varepsilon'(t+\tau, y)\, E'(t, y^{ref})}}{\sqrt{\varepsilon'^2(t, y)}\sqrt{E'^2(t, y^{ref})}}. \tag{3.5}$$

A similar 2-time 2-plane correlation can be defined by replacing TKE with TPR, i.e. E^{ref} with P^{ref}, and E' with P'. From the 2-time 1-plane correlations between TKE and TDR in figures 3(*a*,*c*,*e*,*g*,*i*), we observe a region of low positive correlations between $y/H = 0.2$ and $y/H = 0.4$, the outer part of the near-equilibrium ($\bar{P} \approx \bar{\varepsilon}$) region. We therefore start by plotting the correlation contours for reference plane $y^{ref}/H = 0.3$, which is where the minimal 2-time 1-plane correlation at zero time lag is found (figure 3). Taking a different reference plane within this low correlation region $y/H = 0.2$ to $y/H = 0.4$ changes little the observations that follow throughout the paper.

The correlation contours in (τ, y) space, with TKE at reference plane $y^{ref}/H = 0.3$, are plotted in figure 4 for the five Reynolds numbers considered. It can be observed clearly that the TKE in the near-equilibrium region correlates with the TDR in both the core region and the near-wall region, with a positive time lag and also a wall-distance lag. This observed time lag resolves the discrepancy between volume-averaged correlations and 2-time 1-plane correlations. Along the path of positive correlation from the reference plane towards the channel centre, the peaks of correlations in (τ, y) space lie very close to a line of slope $\delta y/\delta\tau = (1 \pm 0.2)u_\tau$ (see figures 4 and 5*a*). This is a time lag combined with a wall-distance lag, and the ratio of the latter to the former is $\sim u_\tau$. Note that any turbulence transport in the wall-normal direction should be through the wall-normal velocity in the turbulence transport term (see $T_t(y, t)$). The mean wall-normal velocity is zero, but the standard deviation of the wall-normal velocity fluctuations v_{rms} is of order u_τ and varies slowly with y. The correlations with time lag in figure 4 cannot be caused by the passage of inclined structures observed previously in turbulent boundary layers (e.g. in Marusic & Heuer 2007) and FD TCF (e.g. in Cheng, Shyy & Fu 2022). If they were, then TDR in the core region would precede TKE in the near-equilibrium region due to the earlier passage of structures further away from the wall than closer to the wall.

The TKE can be transported both upwards and downwards from the reference plane. During wall-normal turbulence transport, high TKE fluctuations are also transferred towards smaller scales, which leads to high TDR fluctuations. This transport through scales is illustrated by the increasing correlation between TKE and TDR further away from the reference plane (figure 4), as well as by the path of the slowest decorrelation of TKE with itself, which is also along the line of slope $\delta y/\delta\tau \approx u_\tau$ (not shown here). This interpretation is supported by figure 6, which shows that the 2-time 2-plane correlation between TPR and TDR behaves differently even though the volume-averaged TPR has similar time lags with volume-averaged TDR and volume-averaged TKE. The difference between figures 4 and 6 can be understood by using the fact that TPR is not transported through space and scales, whereas TKE is. Figure 6 shows that TPR and TDR are maximally correlated locally rather than non-locally along a $\delta y/\delta\tau$ line as in the case of TKE and TDR in figure 4.

Regarding the path of high correlations towards the core region, the velocity $\delta y/\delta\tau$ is close to that of the plane-averaged ejections found by Flores & Jiménez (2010). In the core region, the mean shear is very weak, and the eddies are composed mainly of dissipative ones (see § 3.2). It is therefore conceivable that this path is associated with the energy cascade initiated from the large-scale structure mainly around $y^{ref}/H = 0.3$. This would

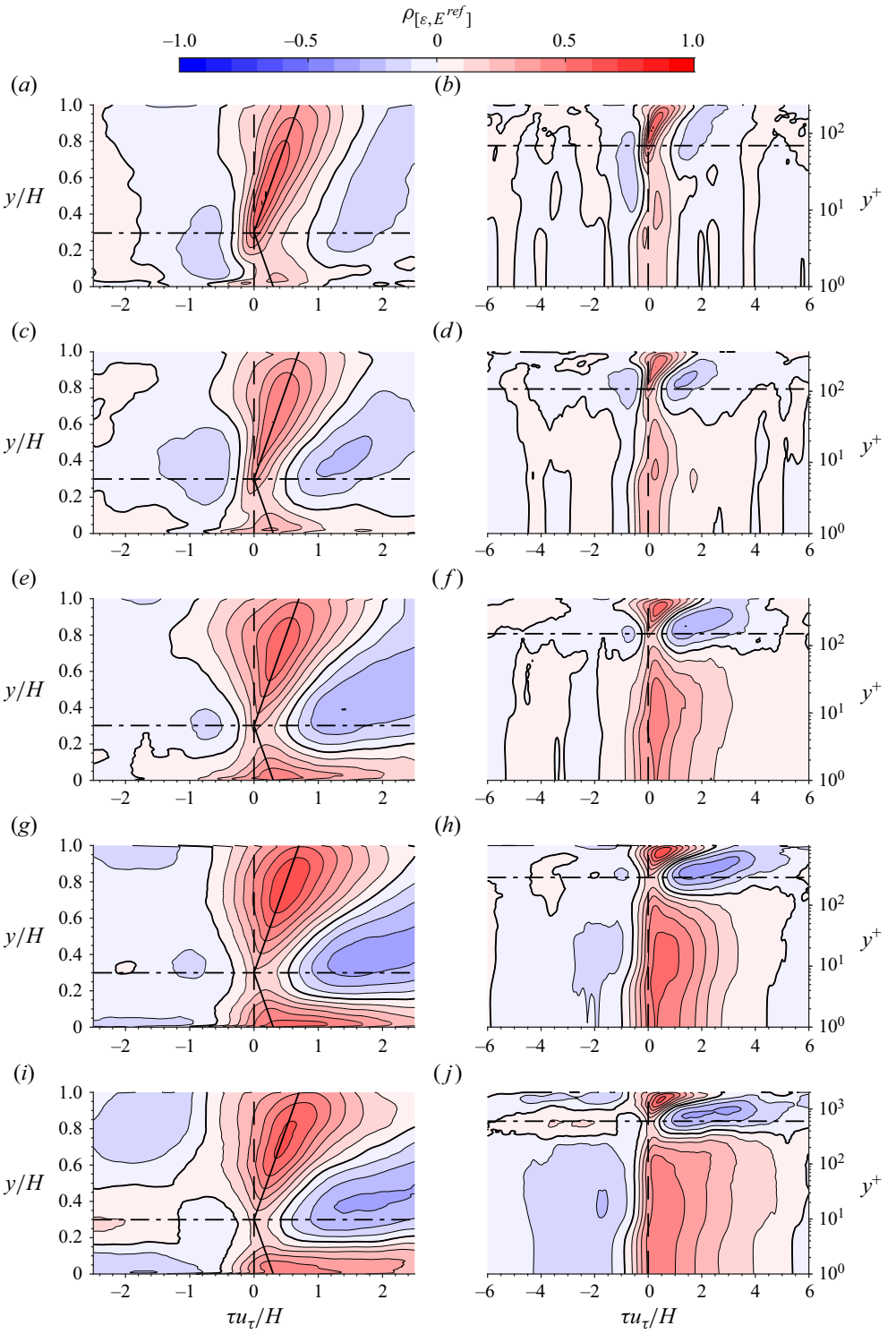

Figure 4. The 2-time 2-plane correlation function contours $\rho_{[\varepsilon,E^{ref}]}$ versus distance from the wall y^+ or y/H and time lag $\tau u_\tau/H$ with respect to TKE at the reference plane $y^{ref}/H = 0.3$ (horizontal dash-dotted lines). The slopes of the solid black lines are $\pm u_\tau$, respectively. Plots for (*a*,*b*) R230, (*c*,*d*) R360, (*e*,*f*) R500, (*g*,*h*) R950, (*i*,*j*) R2000. Vertical dashed lines indicate $\tau = 0$.

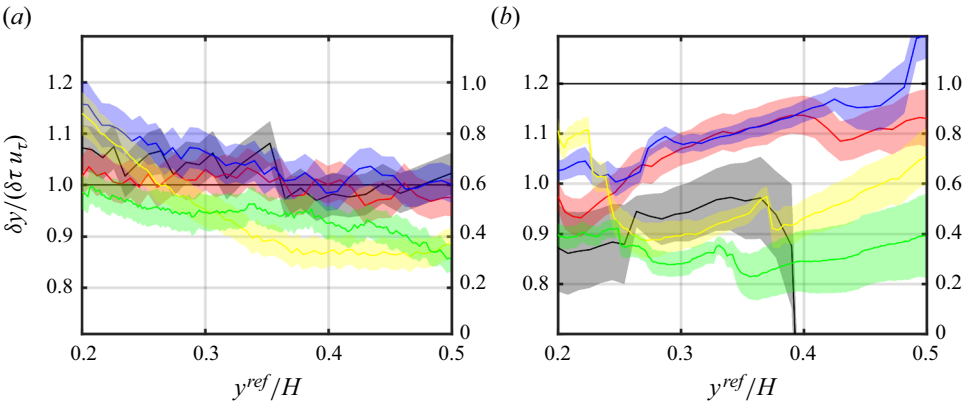

Figure 5. For given y^{ref}, one defines $\delta y(y, y^{ref}) \equiv |y - y^{ref}|$, and then extracts $\delta\tau$ from the maximum correlation at local y and y^{ref}, i.e. $\rho(\delta\tau, y; y^{ref}) = \sup_\tau\{\rho(\tau, y; y^{ref})\}$, where ρ is defined in (3.5). A best linear fit of δy versus $\delta\tau$ gives an average slope $\delta y/\delta\tau$ with its 95 % confidence interval for each y^{ref}. We plot the fitted slopes $\delta y/(\delta\tau u_\tau)$ as a function of y^{ref} (*a*) for the 2-time 2-plane correlations above the reference plane, and (*b*) for the 2-time 2-plane correlations below the reference plane. In both (*a*,*b*), the shadings around the different coloured lines are 95 % confidence intervals for R230 (black line), R360 (red line), R500 (blue line), R950 (yellow line) and R2000 (green line).

also imply that the ejections towards the outer region (Flores & Jiménez 2010) involve not only momentum transport but also energy transport in space and in scales, which leads to TDR fluctuations through a cascade process. In the path towards the wall, the correlation velocity $\delta y/\delta\tau$ appears to be smaller than $(1 \pm 0.2)u_\tau$ and less well-defined (see figure 5*b*). The contours in figure 4 show that as Re_τ increases, the TKE in the near-equilibrium region and the TDR in the near-wall region correlate with a wider and more skewed spread of time lags in H/u_τ units. It is worth emphasising that this TKE to TDR spatio-temporal path towards the wall is fundamentally different from the superposition and modulation effects described in Hutchins & Marusic (2007*b*).

As in § 3.2, we observe from the 2-time 2-plane correlation in figure 4 a region of anti-correlation between TDR and TKE around the reference plane at $y^{ref} = 0.3H$. The extent of this anti-correlation shows a spread of time lags beyond $\tau u_\tau/H \approx 0.5$, and little wall-distance lag, consistent with the anti-correlation in 2-time 1-plane correlation in figure 3. This anti-correlation signifies a high/low TKE event followed in time by low/high dissipation around a reference plane taken at the outer edge of the near-equilibrium region. A plausible explanation for the local anti-correlation between TKE and TDR with time lag could be that TKE is transported away from the upper near-equilibrium region and therefore does not remain there to cascade and dissipate. A high instance of TKE at the upper near-equilibrium region is therefore followed by no increase in dissipation – in fact, even a decrease in dissipation, given that there is no local cascade at $y \approx y^{ref}$ between $y/H = 0.2$ and $y/H = 0.4$ to feed it.

As a side note, unlike the peak of 2-time 1-plane correlation located at the channel centre in figure 3, the maximum 2-time 2-plane correlation reaches only a distance from the wall approximately $y \sim 0.75H$, above which TKE at the reference plane decorrelates with TDR in the core region. This observed decorrelation is likely due to the fact that the single core region in FD TCF contains information such as signals of TKE ejected from both the upper channel and the lower channel. It would be interesting to investigate in the future temporal correlations between TKE in the near-equilibrium layer and TDR in the

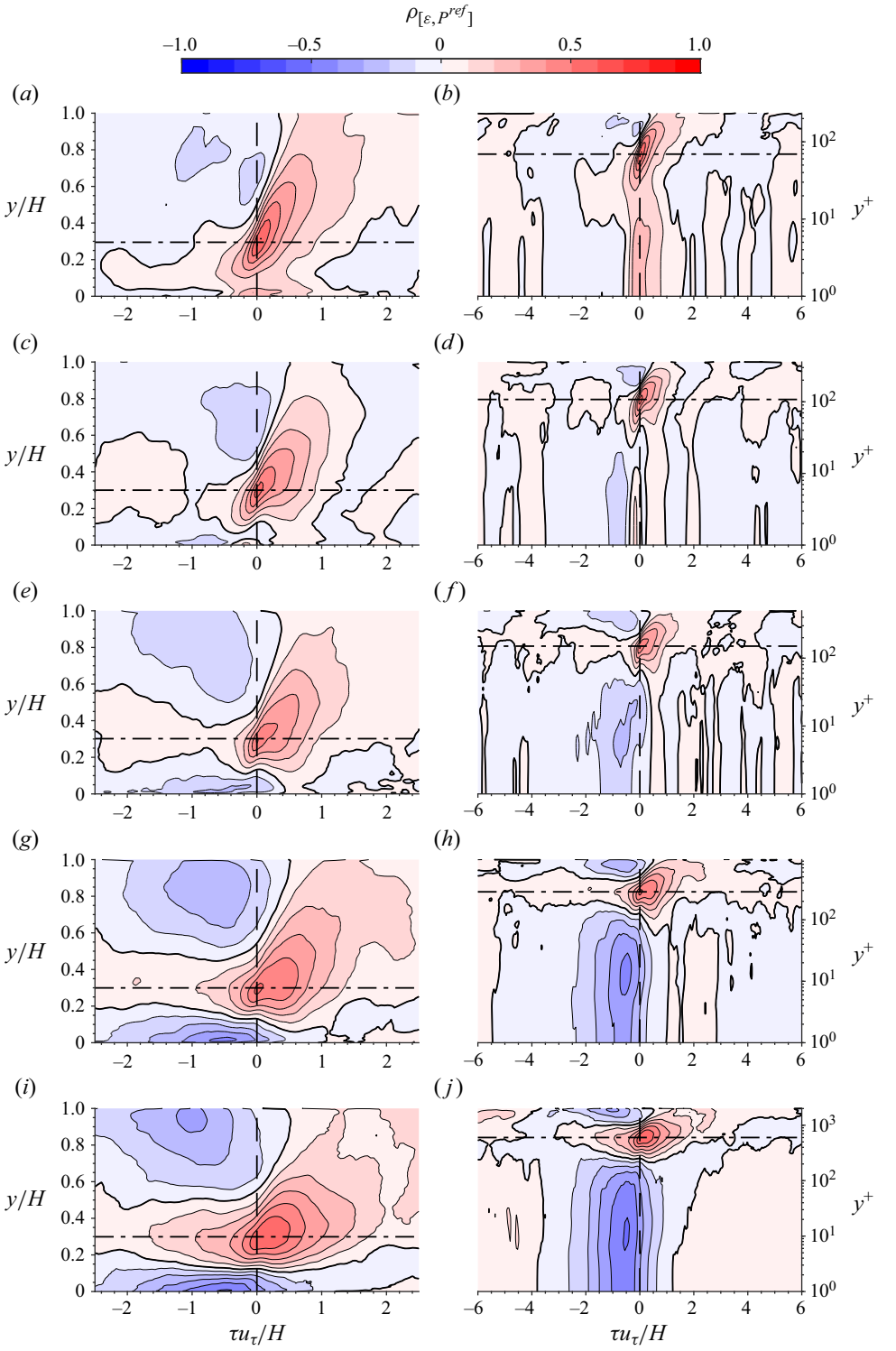

Figure 6. The 2-time 2-plane correlation function contours $\rho_{[\varepsilon,P^{ref}]}$ versus distance from the wall y^+ or y/H and time lag $\tau u_\tau/H$ with respect to TPR at the reference plane $y^{ref}/H = 0.3$ (horizontal dash-dotted lines). Plots are for (*a*,*b*) R230, (*c*,*d*) R360, (*e*,*f*) R500, (*g*,*h*) R950, (*i*,*j*) R2000. Vertical dashed lines indicate $\tau = 0$.

outer layer of wall-bounded turbulence with only one wall, such as that of open channel flow (Yao, Chen & Hussain 2022; Pirozzoli 2023) or turbulent boundary layers.

3.4. *The 2-time 2-plane correlations: near-wall region and Reynolds number dependence*

The observations made in § 3.3 indicate a correlation velocity closely related to the turbulence transport velocities from the near-equilibrium region both towards and away from the wall. The path of correlation away from the wall shows little dependence on the Reynolds number and is always very close to the friction velocity. However, the correlation between the TKE in the near-equilibrium region and the TDR in the near-wall region is heavily dependent on Reynolds number. We therefore turn our focus to the 2-time 2-plane correlations between TKE at a reference plane taken in the near-wall region, and TDR fluctuations elsewhere. The correlation contours with reference plane taken at $y^{ref} = 10\delta_\nu$ are presented in figure 7. This figure does not change significantly if we take a different reference plane in the range $y^{ref} \in [10, 50]\,\delta_\nu$.

The first point made by figure 7 is that TKE and TDR fluctuations are strongly correlated in the near-wall region below $y^+ \approx 100$, without time lag on average, but also, quite symmetrically, with equally positive and negative time lags in the range $-2 \leqslant \tau u_\tau/H \leqslant 2$. This strong correlation makes sense given that the length and velocity scales associated with TKE and TDR are not well separated in the near-wall region. The second observation coming out of figure 7 is that, unlike figure 4, no continuous path of positive correlation exists from the near-wall region to the near-equilibrium region, and ultimately to the core region. And the third observation is the significant positive correlation without significant time lag between TKE in the near-wall region and TDR in the core region.

For a start towards an interpretation of this third observation, we plot in figure 8 the ratio between the time-averaged TPR and the time-averaged TDR in inner and outer units obtained from our data. The notion of 'equilibrium' is merely an approximation of the actual TKE budget in the overlap region. The outer peak of the production to dissipation ratio increases with Reynolds number, and moves away from the wall in inner units. This is a signature of the very-large-scale motions at moderately high Reynolds number (Kim & Adrian 1999). As these outer structures become stronger with increasing Reynolds number, their contributions to the fluctuations in the TKE budget may also become more pronounced. These strong outer structures in the near-equilibrium region become increasingly dominant in both outer and near-wall TDR fluctuations. In the near-wall region, TKE and TDR fluctuate almost in the same manner (as seen from the high correlation with no time lag on average in the near-wall region in figure 7). Strong correlations between TKE near the wall and TDR in the core region therefore also indicate strong correlations between TDR near the wall and TDR in the core region with zero or little time lag at high Reynolds number, both presumably controlled by strong energy-containing structures of sizes comparable to the half-channel height. Indeed, the 2-time 2-plane correlations of TDR at $y^+ = 10$ and TDR at other wall distances y (not shown here for economy of space) are nearly identical to figure 7 except perhaps at the lowest $Re_\tau = 230$, for which they are just very similar. A correlation where the reference TKE is taken in the core region was also computed (not shown here for economy of space), and similar instantaneous correlation values with the near-wall TDR were found, suggesting that the near-wall TDR and the core TDR are both controlled by structures of sizes comparable to the half-channel height.

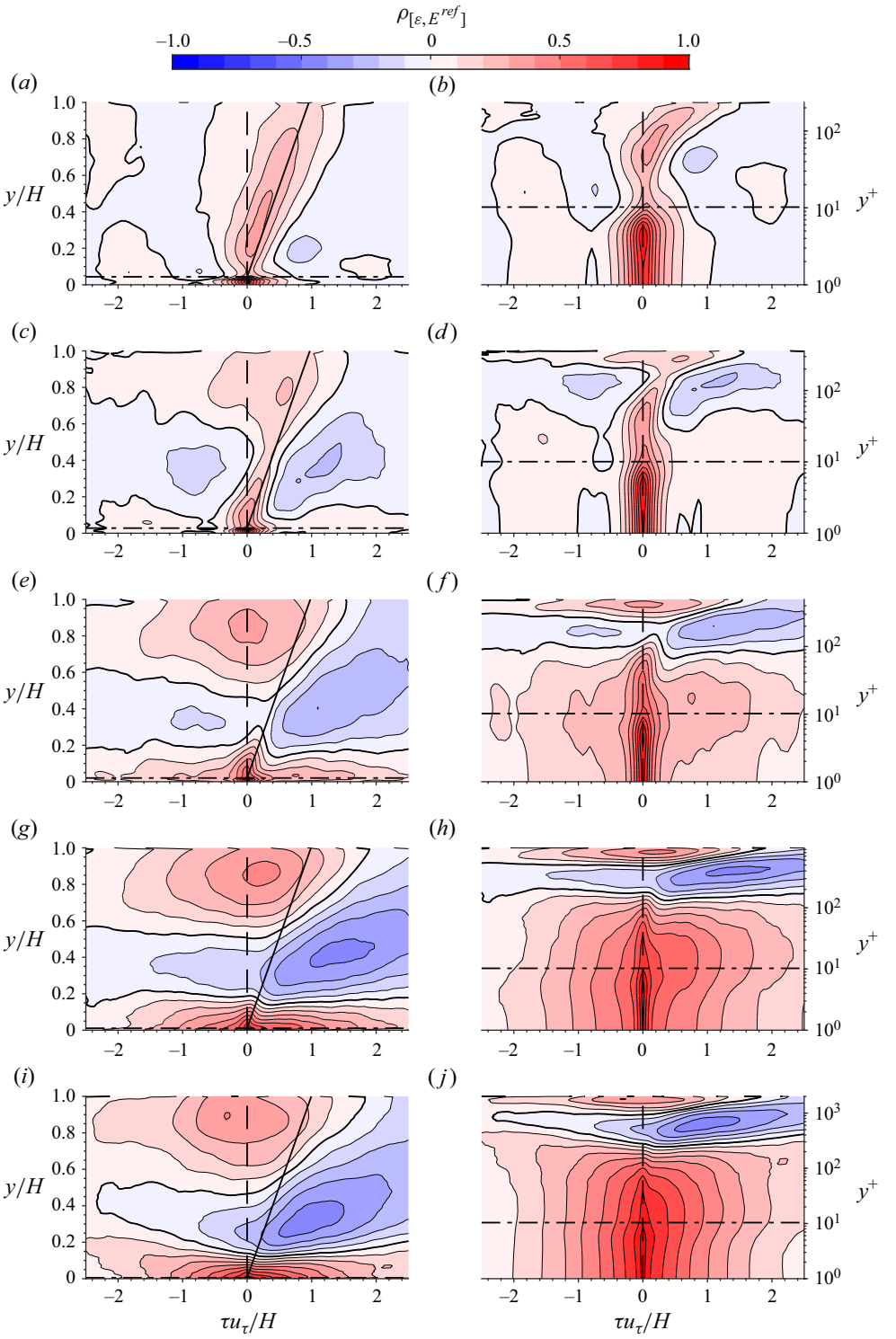

Figure 7. The 2-time 2-plane correlation function contours $\rho_{[\varepsilon,E^{ref}]}$ versus distance from the wall y^+ or y/H and time lag $\tau u_\tau/H$ with respect to TKE at the reference plane $y^{ref} = 10\delta_v$ (horizontal dash-dotted lines). The slopes of the solid black lines are $\pm u_\tau$, respectively. Plots are for (*a*,*b*) R230, (*c*,*d*) R360, (*e*,*f*) R500, (*g*,*h*) R950, (*i*, *j*) R2000. Vertical dashed lines indicate $\tau = 0$.

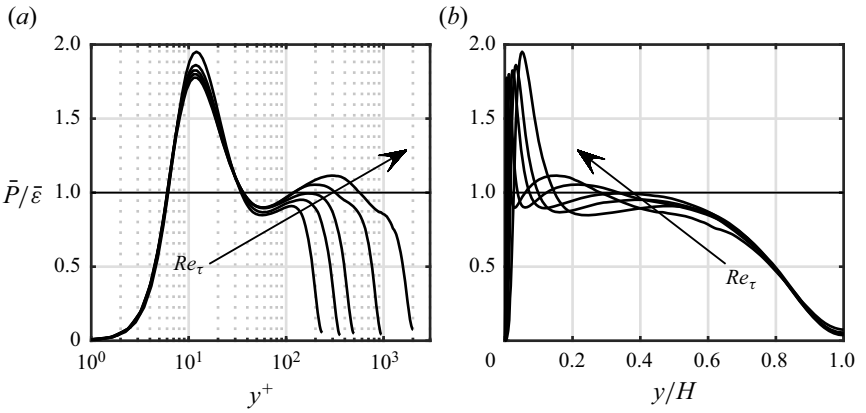

Figure 8. Time-averaged mean profile of TPR over TDR in (*a*) inner units and (*b*) outer units for five Reynolds numbers. Horizontal solid line indicates $\bar{P}/\bar{\varepsilon} = 1$.

3.5. *The 2-time 2-plane correlations: ejections and sweeps*

As already mentioned in § 3.3, the spatio-temporal path of TKE to TDR from the near-equilibrium region to the outer region observed in that subsection is reminiscent of the spatio-temporal path of ejections/sweeps observed by Flores & Jiménez (2010). Hence we now focus on the regions in the x–z plane where ejections and sweeps happen. For any quantity $Z(x, y, z, t)$ in FD TCF, we define a conditional plane average as

$$Z_{Qs}(y, t) = \frac{1}{A_{Qs}(y, t)} \iint_{Qs} Z(x, y, z, t)\, \mathrm{d}x\, \mathrm{d}z, \tag{3.6}$$

where Qs, for $s = 1, 2, 3, 4$, indicates the four quadrants in the u–v plane, and $A_{Qs} = A_{Qs}(y, t)$ is the sum of the areas in the x–z plane where Qs events take place (Wallace *et al.* 1972; Willmarth & Lu 1972). In particular, we investigate 2-time 2-plane correlations of unconditioned TDR with TKE conditionally averaged either over ejections (Q2) or over sweeps (Q4) in each plane. It is well-known that ejections and sweeps are the principal contributors to the Reynolds stress $-\langle u'v' \rangle$ in the near-equilibrium region (Willmarth & Lu 1972).

Figure 9 presents the same correlation function as in (3.5), but using unconditioned TDR and TKE conditionally averaged (as in (3.6)) over Q2 ejection events, i.e. locations in the plane where $u' < 0$ and $v' > 0$. The resulting correlation contours show a trend consistent with the unconditional TKE and TDR in figure 4 (in particular, very similar correlation velocities $\delta y/\delta\tau$ to within 10 %, and correlation levels comparable to the unconditional correlations to within 7 %).

When the correlation function is computed using TKE conditionally averaged over Q4 sweep events ($u' > 0$ and $v' < 0$) as shown in figure 10, noticeable changes in the correlation velocity and in the values of correlation coefficients appear. The spatio-temporal path towards the core region shows a significantly reduced correlation velocity (by up to 33 %) and significantly reduced levels of correlation (by up to 20 %). The perhaps counter-intuitive observation, however, is the difference of the correlation coefficients between the ejection-conditioned and sweep-conditioned correlations in the near-wall region. Sweep events are $v' < 0$ events, which in effect transport high streamwise momentum ($u' > 0$) towards the wall. They may therefore be expected to be mainly responsible for the dissipation of the near-wall region, hence the TKE and

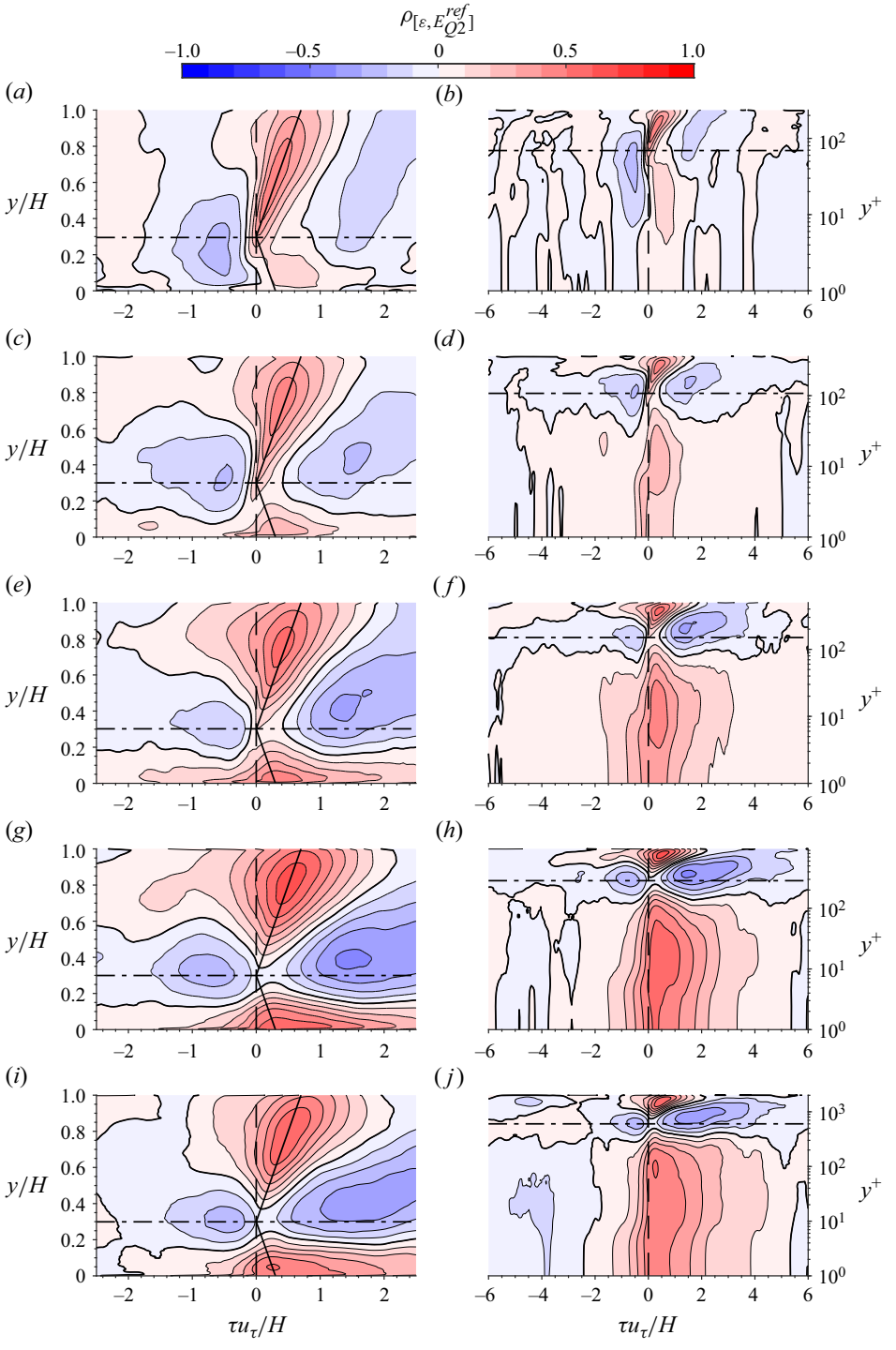

Figure 9. The 2-time 2-plane correlation function contours $\rho_{[\varepsilon,E_{Q2}^{ref}]}$ versus distance from the wall y^+ or y/H and time lag $\tau u_\tau/H$ with respect to TKE conditioned on ejection events at the reference plane $y^{ref}/H = 0.3$ (horizontal dash-dotted lines). The slopes of the solid black lines are $\pm u_\tau$, respectively. Plots are for (*a*,*b*) R230, (*c*,*d*) R360, (*e*,*f*) R500, (*g*,*h*) R950, (*i*,*j*) R2000. Vertical dashed lines indicate $\tau = 0$.

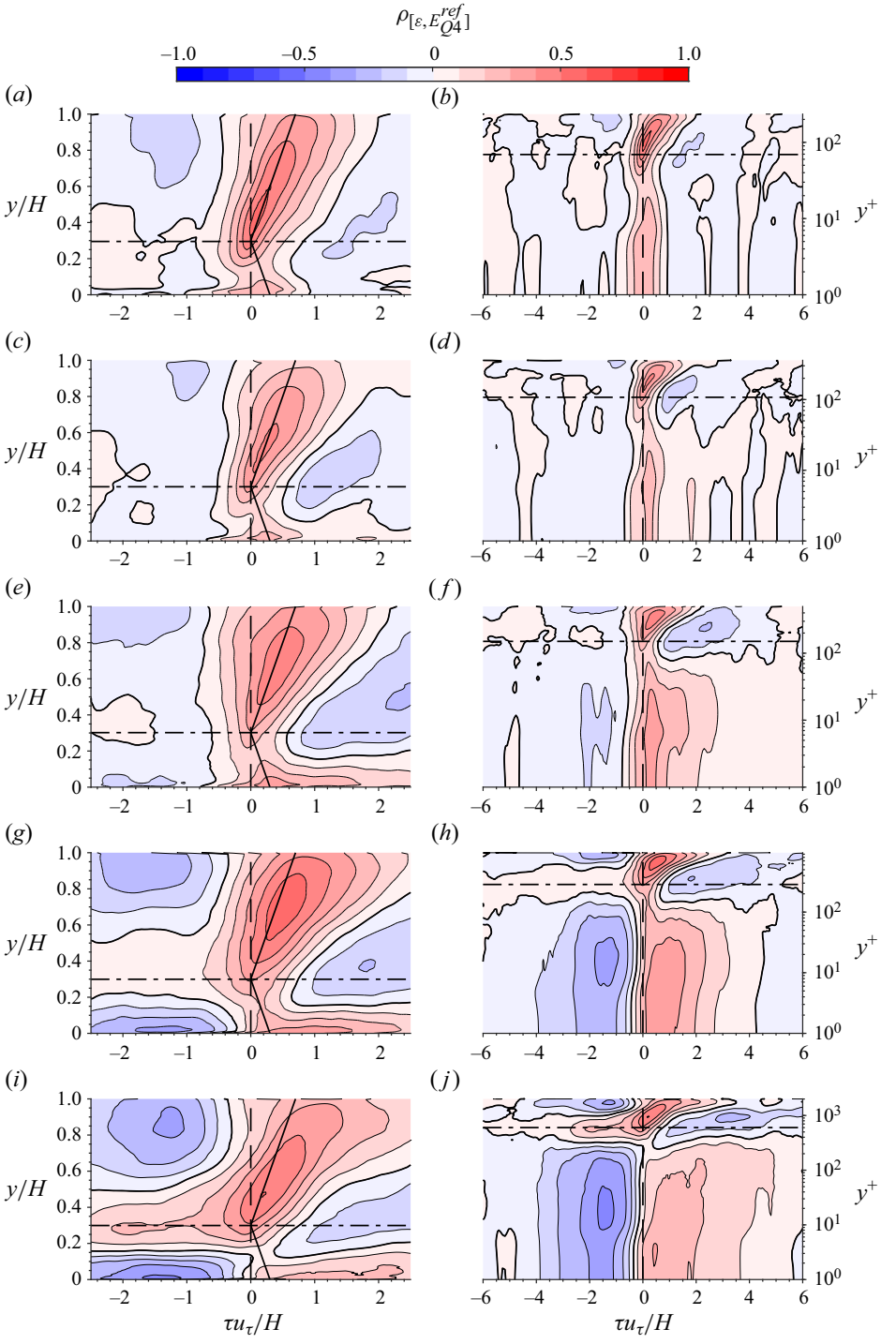

Figure 10. The 2-time 2-plane correlation function contours $\rho_{[\varepsilon,E_{Q4}^{ref}]}$ versus distance from the wall y^+ or y/H and time lag $\tau u_\tau/H$ with respect to TKE conditioned on sweep events at the reference plane $y^{ref}/H = 0.3$ (horizontal dash-dotted lines). The slopes of the solid black lines are $\pm u_\tau$, respectively. Plots are for (*a*,*b*) R230, (*c*,*d*) R360, (*e*,*f*) R500, (*g*,*h*) R950, (*i*,*j*) R2000. Vertical dashed lines indicate $\tau = 0$.

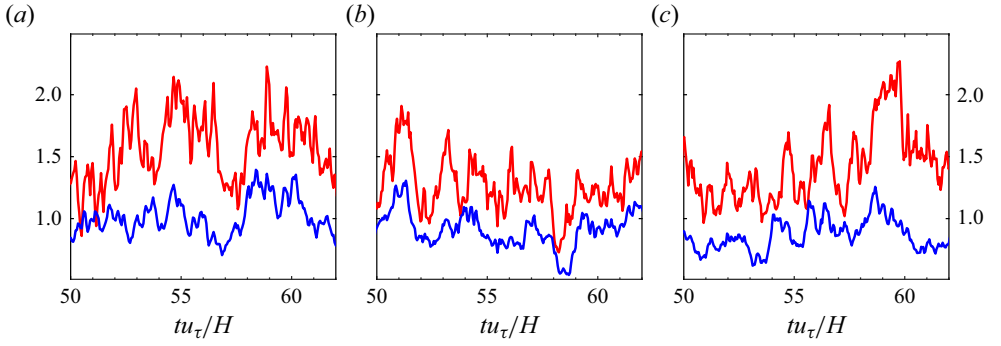

Figure 11. Time evolution of conditionally averaged TKE $E_{Qs}/\bar{E}$ at $y/H = 0.3$, normalised by plane- and time-averaged TKE, in the lower half-channel. Red signals indicate TKE conditionally averaged over ejections ($s = 2$), and blue over sweeps ($s = 4$). Plots are for (*a*) R500, (*b*) R950, (*c*) R2000.

TDR conditionally averaged over sweep events may be expected to be more strongly correlated with higher correlation coefficient near the wall. The present correlation contours are contrary to this expectation. Even though ejection events correspond to $v' > 0$ structures that would mainly transport slow ($u' < 0$) streamwise momentum away from the wall, they appear to be better correlated with the near-wall dissipation than sweep events. For the higher three Reynolds numbers, the correlation levels between reference ejection-conditioned TKE and near-wall TDR (figures 9*f*,*h*,*j*) vary within 10 % of the unconditional correlation (figures 4*f*,*h*,*j*), whereas the sweep-conditioned correlation levels (figures 10*f*,*h*,*j*) are reduced by 20 %–36 %.

In FD TCF, the plane-averaged wall-normal velocity must satisfy $\langle v \rangle (y, t) = 0$, an exact result imposed by the no-penetration boundary condition, homogeneity in the wall-parallel directions and incompressibility. This suggests that locally positive $v' > 0$ and negative $v' < 0$ must occur in pairs at any wall-parallel plane in the channel. As a result, ejections and sweeps should also happen simultaneously at any plane, and the TKE conditionally averaged over ejections and sweeps should fluctuate more or less concurrently, as appears to be approximately the case (see figure 11). On the other hand, it is worth pointing out that ejections have previously been shown to provide the largest contribution to the overall Reynolds shear stress and TKE (Willmarth & Lu 1972). From figure 11, in the near-equilibrium region, the TKE conditionally averaged over ejections is indeed higher than conditionally averaged over sweeps, indicating that local turbulent motions associated with ejections are more energetic than sweeps (Farano *et al.* 2017), which might be responsible for the faster correlation velocity than that of sweeps towards the core region.

In the near-wall region, there is little separation between energy containing length scales and dissipative length scales. Turbulence energetics, whether the TKE or dissipation, plane-averaged or conditionally averaged over ejections/sweeps, are expected to fluctuate concurrently near the wall. While we expect the sweeps to be responsible for the near-wall fluctuations, it is actually the ejections in the near-equilibrium regions that correlate with the near-wall dissipation better, contrary to our expectation. We present here a hypothesis to account for this observation. As ejections and sweeps operate in tandem, anything relating to one should also somehow relate to the other. Presumably, sweeps are responsible for the connection and travel to the wall, and ejections for the connection and travel to the core, but correlations conditioned on ejections are stronger than correlations conditioned on sweeps because ejections are more organised/structured

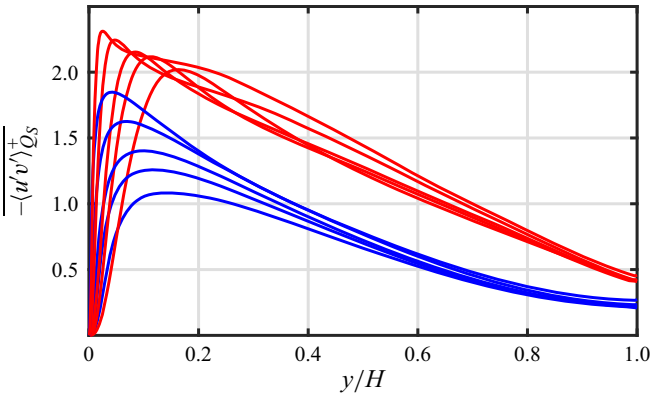

Figure 12. Time-averaged mean profile of conditionally averaged Reynolds shear stress over ejections (red lines) and sweeps (blue lines) for five Reynolds numbers.

than sweeps. In support of this suggestion, we plot in figure 12 the time-averaged mean profile of conditionally plane-averaged Reynolds shear stress over ejections and over sweeps, respectively. One may consider the Reynolds shear stress as an indication of organisation/coherence given that $-\langle u'v'\rangle = 0$ if u' and v' are uncorrelated, as expected in the absence of organised coherent flow structure, and therefore higher absolute values of $-\langle u'v'\rangle$ indicate higher order/coherence. In the case of FD TCF, the magnitude of $\overline{-\langle u'v'\rangle_{Q2}}$ (time-averaged $-\langle u'v'\rangle$ conditioned on Q2, i.e. plane-averaged over Q2 regions only) is significantly larger than $\overline{-\langle u'v'\rangle_{Q4}}$ for $y > 0.2H$, thereby suggesting that ejections are more organised than sweeps. As a result, the correlations conditioned on ejections in figure 9 are stronger than the correlations conditioned on sweeps in figure 10, both towards the wall and towards the core. Note that significant correlations conditioned on sweeps also appear towards the core region in figure 10, which is as counter-intuitive as the significant correlations conditioned on ejections towards the wall in figure 9.

4. Dynamics of TPR

Having examined the links between TKE and TDR fluctuations we now turn to the production of TKE which, anyway, occurs before its dissipation. Of course, one expects the volume-averaged TPR to lead the volume-averaged TKE simply because TKE builds up as an integration in time of TPR (see (3.2)). This is confirmed by the cross-correlation function $\rho_{[P_V,E_V]}$ (red line in figures 1*c*,*f*,*i*,*l*,*o*): the peaks of the correlations are at approximately $\tau u_\tau/H \sim -0.1$ (time lead) with values of $\rho_{[P_V,E_V]}$ between 0.5 and 0.8 (increasing with Re_τ). The 2-time 1-plane correlation $\rho_{[P,E]}$ (not shown here for brevity), calculated as in (3.4) by replacing TDR ε with TPR P, shows little/no average time lag between the plane-averaged TPR and the plane-averaged TKE, suggesting that the dynamic relation between TPR and TKE is more complex than expected.

In § 4.1, we therefore investigate the 2-time 2-plane correlation $\rho_{[P,E^{ref}]}$ between TKE at reference plane $y^{ref}/H = 0.3$ (chosen indicatively as results are very similar for any y^{ref}/H between 0.2 and 0.4) and TPR elsewhere. The TPR fluctuations result from fluctuations of mean shear and Reynolds shear stress, and we therefore concentrate on both in §§ 4.2 and 4.3. A mechanistic model is proposed in § 4.3 to explain the dynamics relating TPR and TKE.

4.1. *The 2-time 2-plane correlation: TPR and TKE*

We plot in figure 13 the 2-time 2-plane correlation between TKE at reference plane $y^{ref} = 0.3H$ and TPR elsewhere. Positive correlations exist between TKE at the reference plane and TPR in the near-wall and TPR in the core region. The correlations in the core region share peak locations similar to those between TKE and TDR (figure 4), but the levels of correlation between TKE and TPR are significantly lower, and the correlation peaks do not follow the $\delta y/\delta\tau \approx u_\tau$ line that characterises the path from TKE to TDR. The core correlation between TKE and TPR must be rooted in the correlation between TKE and Reynolds shear stress (see § 4.2).

The positive correlations between TKE at the reference plane and TPR in the near-wall region appear similar to the correlations between TKE at the same reference plane and TDR in the near-wall region (see figure 4) in terms of both the levels of correlations and the peak locations of the correlations, i.e. the average time lags. As discussed in §§ 3.2, 3.4 and 3.5, the near-wall dynamics are limited by a small range of scales, and TKE, TDR and TPR fluctuate almost concurrently near the wall. The similarity between correlations $\rho_{[P,E^{ref}]}$ and $\rho_{[\varepsilon,E^{ref}]}$ near the wall is therefore expected. One observation is that the near-wall production depends on the turbulent energy further away from the wall, which becomes more evident at higher Reynolds numbers (increasing levels of correlation in the near-wall region). The peaks of the correlation with time lag instead of time lead indicate that the near-wall TPR lags the reference TKE. Such an observation may be unexpected, since one often views the turbulence production as a source of turbulent energy, and TPR should lead TKE in time, as shown in a volume average sense in § 3.1.

It is worth pointing out that the 2-time 2-plane correlations with time lags in figure 13 are not inconsistent with the time lead of peak $\rho_{[P_V,E_V]}$ observed in the volume-averaged correlation. The observed positive values in figure 13 of 2-time 2-plane correlations with time lag in the near-wall and core regions largely cancel the negative values of 2-time 2-plane correlations with time lag in the near-equilibrium region when integrated in the wall-normal direction, and the overall time-lagged peaks of correlations are attenuated.

4.2. *The 2-time 2-plane correlation: Reynolds shear stress and TKE*

The time-fluctuating TPR is the product of the time-fluctuating plane average mean streamwise shear and the time-fluctuating plane-averaged Reynolds shear stress $-\langle u'v'\rangle$. (The contribution from the plane-averaged spanwise mean shear and the corresponding Reynolds shear stress component $-\langle u'w'\rangle$ is minimal compared to the streamwise component, i.e. less than 1 % of the overall production.) We therefore analyse the dynamics of the turbulence production in terms of 2-time 2-plane correlations between TKE at the reference plane and these two factors.

The TKE and the Reynolds shear stress are closely related to each other in terms of their time fluctuations. As shown by the correlation plot $\rho_{[-\langle u'v'\rangle,E^{ref}]}$ in figure 14, the TKE and the Reynolds shear stress are maximally correlated around the reference plane with no average time lag. The correlation contours above the reference plane show both wall-distance lag and time lag along a line of slowest decorrelation that is very close to the friction velocity up to approximately $y = 0.8H$. In the near-wall region around the viscous sublayer, as Reynolds number increases, positive correlations develop with time lag, the spread of which widens in outer time unit H/u_τ, and the levels of correlations increase.

Comparing the correlation contours around the reference plane between $\rho_{[P,E^{ref}]}$ in figure 13 and $\rho_{[-\langle u'v'\rangle,E^{ref}]}$ in figure 14, TKE is strongly correlated with the local Reynolds shear stress, whereas it is relatively decorrelated with TPR. The difference between the

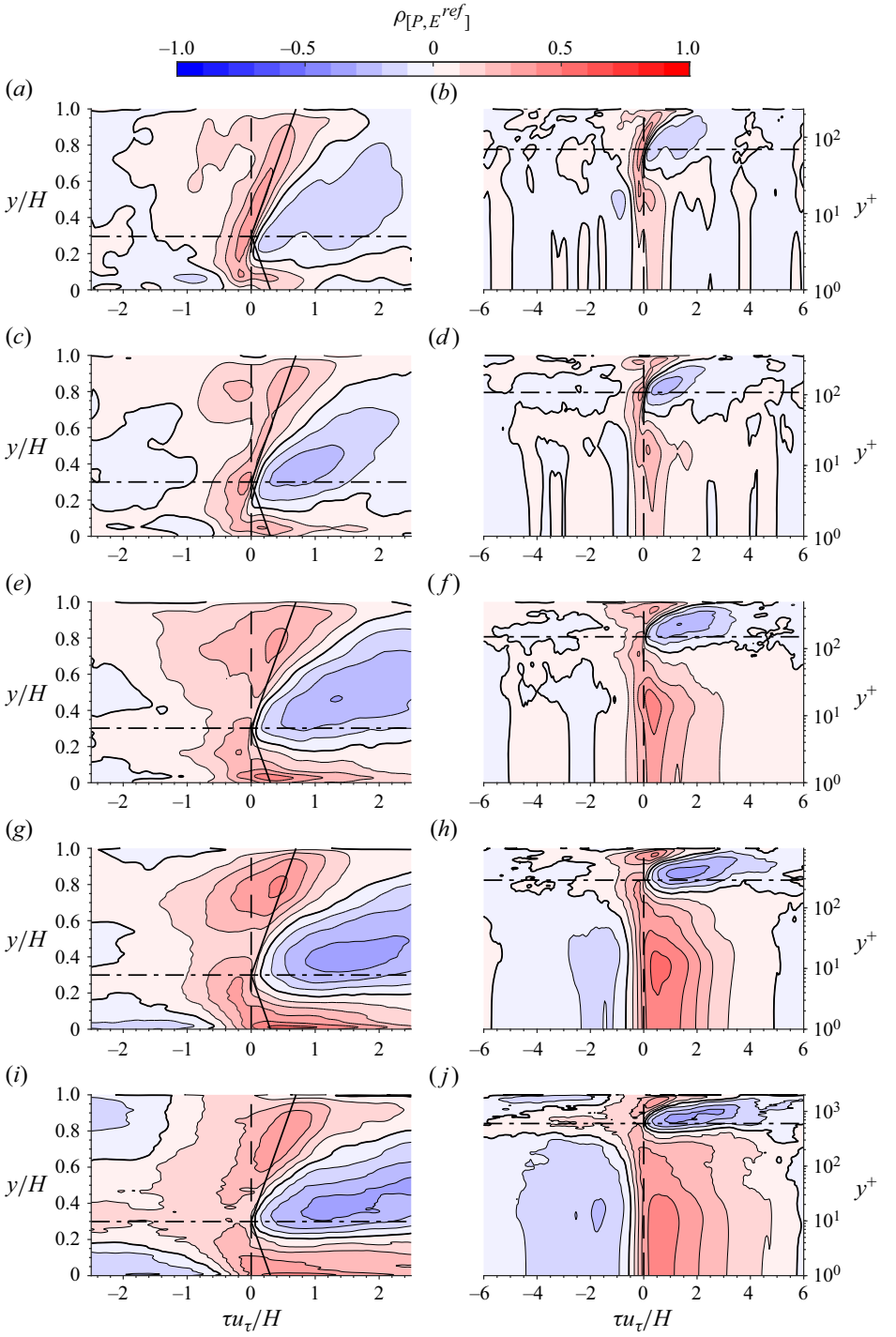

Figure 13. The 2-time 2-plane correlation function contours $\rho_{[P,E^{ref}]}$ versus distance from the wall y^+ or y/H and time lag $\tau u_\tau/H$ with respect to TKE at the reference plane $y^{ref}/H = 0.3$ (horizontal dash-dotted lines). The slopes of the solid black lines are $\pm u_\tau$, respectively. Plots are for (*a*,*b*) R230, (*c*,*d*) R360, (*e*,*f*) R500, (*g*,*h*) R950, (*i*,*j*) R2000. Vertical dashed lines indicate $\tau = 0$.

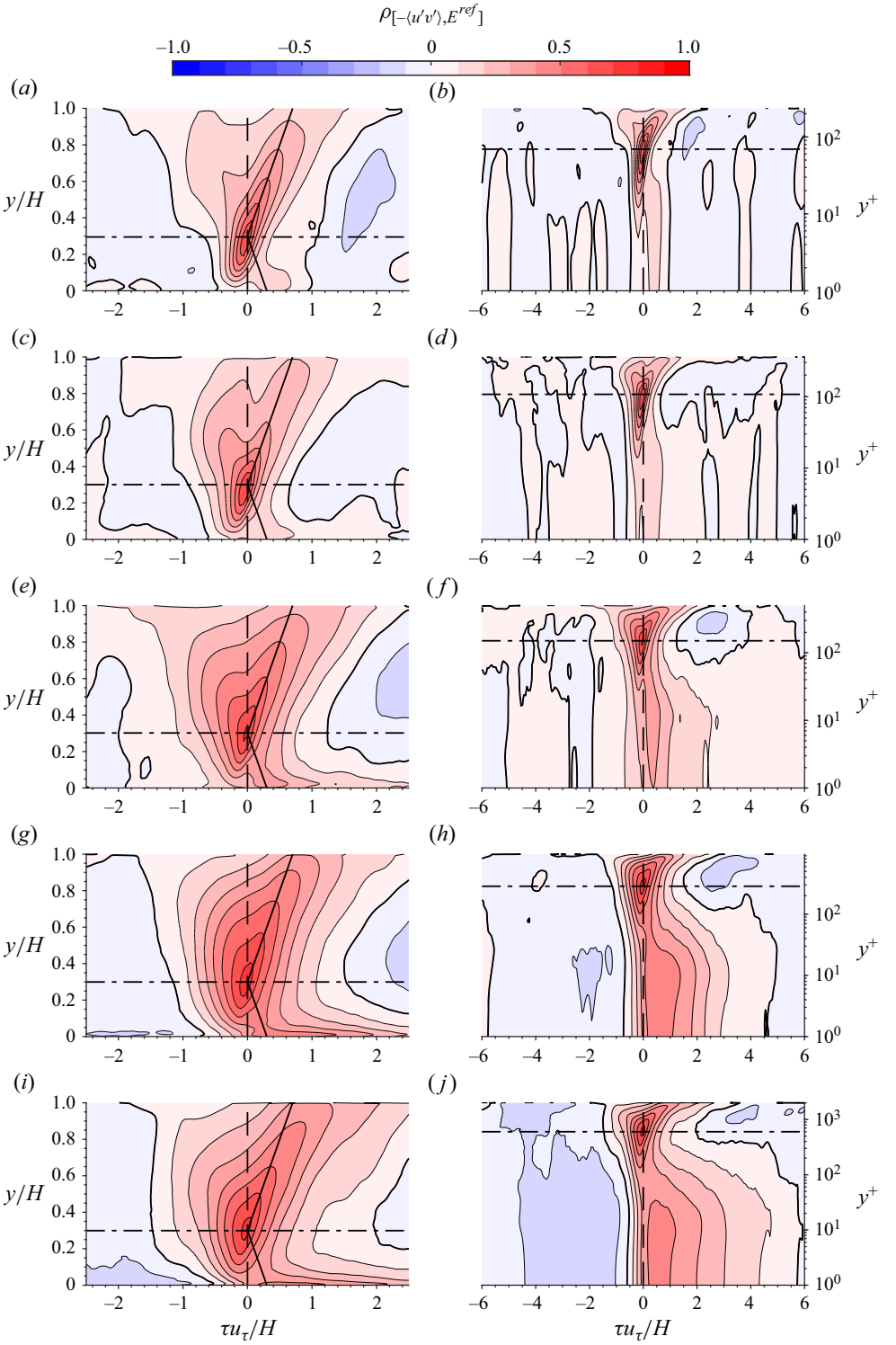

Figure 14. The 2-time 2-plane correlation function contours $\rho_{[-\langle u'v'\rangle, E^{ref}]}$ versus distance from the wall y^+ or y/H and time lag $\tau u_\tau/H$ with respect to TKE at the reference plane $y^{ref}/H = 0.3$ (horizontal dash-dotted lines). The slopes of the solid black lines are $\pm u_\tau$, respectively. Plots are for (*a*,*b*) R230, (*c*,*d*) R360, (*e*,*f*) R500, (*g*,*h*) R950, (*i*,*j*) R2000. Vertical dashed lines indicate $\tau = 0$.

above two correlation contours must be due to the time-fluctuating mean shear. If a time- and plane-averaged mean flow was used, then the plane-averaged mean shear would show no fluctuations in time, and the correlation contours $\rho_{[P,E^{ref}]}$ in figure 13 and $\rho_{[-\langle u'v'\rangle,E^{ref}]}$ in figure 14 would be identical. The dynamics of the plane-averaged mean shear is therefore indispensable for the dynamics of TPR.

4.3. *Interplay between the Reynolds shear stress and the mean shear: a mechanistic model*

To reveal the dynamics of the plane-averaged mean shear and its relation with the plane-averaged Reynolds shear stress, we plot in figure 15 the correlation between the Reynolds shear stress at the reference plane $y^{ref} = 0.3H$ and the mean shear elsewhere. (As already mentioned, the results for $y^{ref} = 0.3H$ are indicative of any y^{ref} between 0.2 and 0.4.) Very similar, if not near-identical, correlation maps (not shown here for brevity) are obtained for the correlation between TKE at the reference plane $y^{ref} = 0.3H$ and the mean shear elsewhere. Around the reference plane, there exists a region of anti-correlation between plane-averaged Reynolds shear stress and mean shear with a spread of time lags. On the other hand, the mean shear in the near-wall region shows a positive correlation with the plane-averaged reference Reynolds shear stress in the near-equilibrium region. High/low TKE or Reynolds shear stress in the near-equilibrium region are followed with some time lag by low/high mean shear in the same region, and by high/low mean shear fluctuations in the near-wall region. The anti-correlation of $\rho_{[\mathrm{d}U/\mathrm{d}y,-\langle u'v'\rangle^{ref}]}$ in the near-equilibrium region in figure 15 resolves the discrepancy between anti-correlation in the contours of $\rho_{[P,E^{ref}]}$ with time lag and $\rho_{[-\langle u'v'\rangle,E^{ref}]}$.

The above observations may be interpreted by the following mechanistic model. Around the near-equilibrium region, when strong ejections and/or sweeps occur, high streamwise momentum in the outer region is transported towards the wall by sweeps, and low streamwise momentum in the inner region is transported away from the wall by ejections, resulting in a local flattening of the mean velocity profile and reduction of the mean shear $\mathrm{d}U(y,t)/\mathrm{d}y$. Therefore, in the near-equilibrium region where viscosity plays little role, high values of $-\langle u'v'\rangle$, and therefore also TKE, precede low values of $\mathrm{d}U/\mathrm{d}y$, as well as resulting reduced values of TPR around the same x–z plane. When high momentum in the outer region is transported to the near-wall region by sweeps, the overall near-wall momentum increases, while the no-slip boundary condition at the wall is unaltered. As a result, the mean shear close to the wall becomes elevated, thereby explaining our observation of a positive correlation with positive time lag between $-\langle u'v'\rangle$ in the near-equilibrium region and $\mathrm{d}U/\mathrm{d}y$ in the near-wall region. Since both the near-wall Reynolds shear stress and the near-wall mean shear are positively correlated with reference TKE in the near-equilibrium region with time lag, the near-wall TPR is also positively correlated with TKE in the near-equilibrium region as in figure 13. This mechanistic model therefore explains how TKE can precede TPR even though volume-averaged TPR obviously precedes, albeit slightly, TKE.

5. Conclusion

Dynamical interactions between turbulent energetics, specifically turbulent kinetic energy (TKE), turbulence dissipation rate (TDR) and turbulence production rate (TPR), have been studied in fully developed turbulent channel flow using temporal correlations at Reynolds numbers up to $Re_\tau \approx 2000$. By using a minimal computational domain

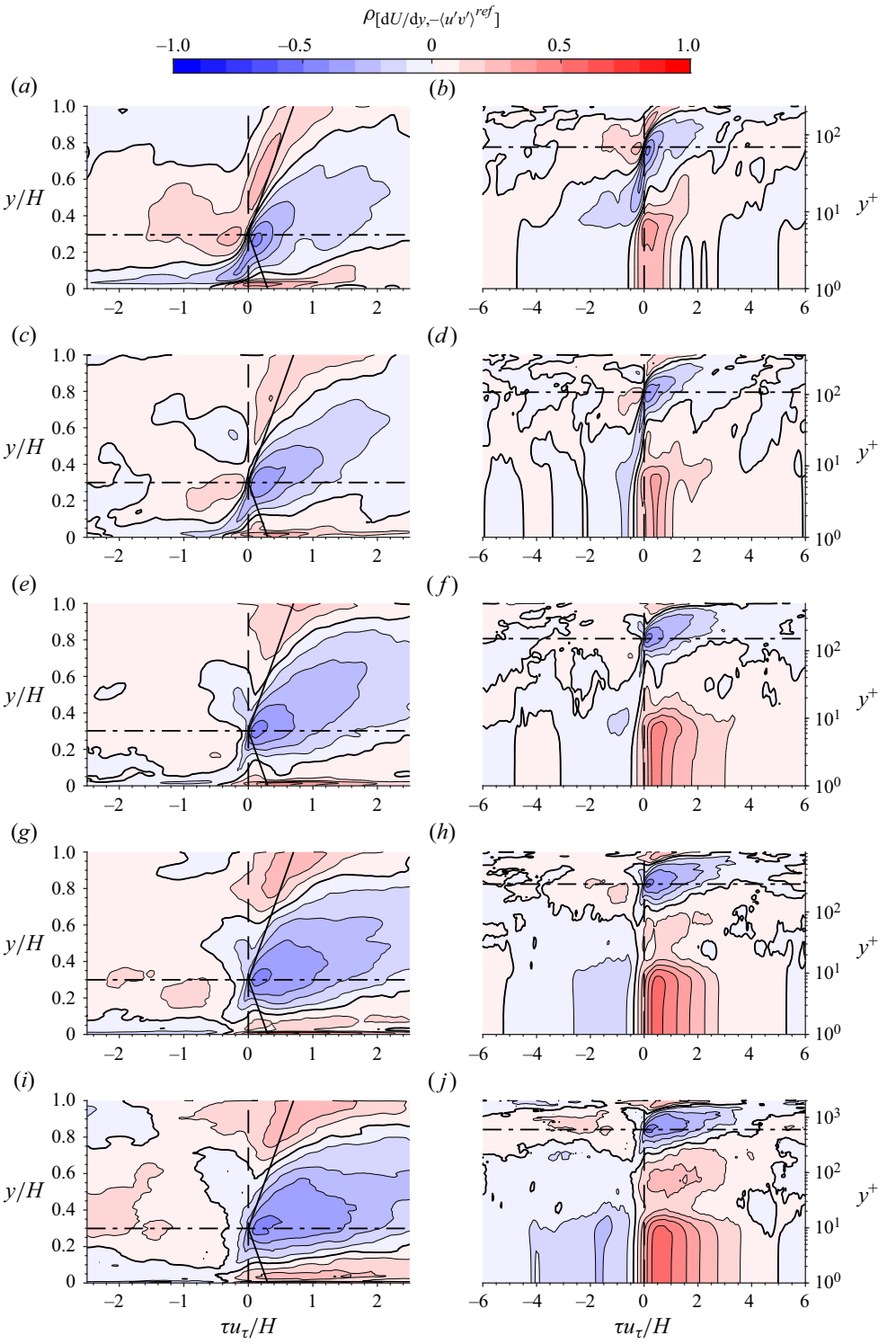

Figure 15. The 2-time 2-plane correlation function contours $\rho_{[dU/dy,-\langle u'v'\rangle^{ref}]}$ versus distance from the wall y^+ or y/H and time lag $\tau u_\tau/H$ with respect to plane averaged Reynolds shear stress at the reference plane $y^{ref}/H = 0.3$ (horizontal dash-dotted lines). The slopes of the solid black lines are $\pm u_\tau$, respectively. Plots are for (*a*,*b*) R230, (*c*,*d*) R360, (*e*,*f*) R500, (*g*,*h*) R950, (*i*,*j*) R2000. Vertical dashed lines indicate $\tau = 0$.

capable of capturing the outer large-scale structures (Hwang & Cossu 2010), volume- and plane-averaged statistics fluctuate in time. For example, plane-averaged fields fluctuate in time, though of course less than fluctuating fields obtained by a Reynolds decomposition and therefore fluctuating around respective plane-averaged fields.

The volume-averaged TKE is found to be correlated with TDR at a later time (i.e. time lag) as in periodic/homogeneous turbulence (Goto & Vassilicos 2015) where this time lag was recognised as resulting from the turbulence energy cascade. The volume-averaged TPR is correlated with TKE at a later time simply because TPR is an energy input rate.

Moving to plane-averaged TKE, TDR and TPR at various wall-normal locations, correlations between plane-averaged TKE and TDR at the same plane reveal almost zero time lag/lead throughout the channel (as in Apostolidis *et al.* 2022). The volume-averaged time lag between TKE and TDR must therefore result from non-local processes in the wall-normal direction.

Non-local correlations are then investigated with 2-time 2-plane correlations, i.e. correlations between plane-averaged TKE at a reference plane in the outer near-equilibrium region (where a local minimum in the 2-time 1-plane correlation is found between TKE and TDR) and plane-averaged TDR at another plane. Positive correlations between reference plane TKE and core region TDR have been revealed with positive time lags $\delta\tau$ and wall-distance lags δy related by $\delta y/\delta\tau \approx u_\tau$ for all Reynolds numbers. There is therefore a correlation path from TKE at the outer near-equilibrium region to TDR in the core that is reminiscent of the momentum transport path by ejections (Flores & Jiménez 2010).

Another path of positive correlation between reference plane TKE and near-wall region TDR has also been found with correlation velocities $\delta y/\delta\tau$ significantly smaller than u_τ, and less well-defined. The path towards the near-wall region shows an increasing spread of time lags with increasing Reynolds number, as also, in fact, observed in the correlation between volume-averaged TKE and TDR. This is a mechanism by which turbulence in the outer part of the near-equilibrium layer influences/controls near-wall TKE, TDR and TPR in a way that involves elevation of production/dissipation throughout the overlap and buffer layers. This mechanism is very different from the superposition and modulation effect described in Hutchins & Marusic (2007*b*), but is reminiscent of a similar effect seen by Doohan *et al.* (2022) at much lower Reynolds number.

A plane-local anti-correlation also exists between TKE and TDR in the same plane within the near-equilibrium region with time lag (from TKE to TDR). This anti-correlation signifies high/low TKE preceding low/high TDR around the reference plane. If the principal mechanism of depletion of local TKE occurs along the two spatio-temporal paths identified in the two preceding paragraphs, so that high TDR follows high TKE along these paths, then little amounts of TKE will be left on the reference plane, thereby leading to relatively low TDR on that plane at later times.

Taking a reference plane near the wall rather than in the outer part of the near-equilibrium region leads to significant instantaneous correlations between near-wall TKE and core region TDR as well as near-wall TDR and core region TDR. This observation points to an additional effect, which may be that near-wall and core region TDR are both controlled in a synchronised way by large energy-containing structures with sizes comparable to the half-channel height.

The relevance of ejections/sweeps to TKE transport has been studied by calculating plane-averaged TKE conditionally on ejections/sweeps. Ejection-based TKE correlates with TDR in a way similar to the unconditional TKE in terms of both the correlation velocity and levels of correlations, whereas the sweep-based TKE is significantly less

correlated with TDR. It is hypothesised that the correlation is higher when conditioning plane-averaged TKE on ejections rather than sweeps along both paths towards the core and towards the wall because ejections have higher absolute values of Reynolds shear stress and are therefore better organised than sweeps.

While the volume-averaged TPR evidently precedes TKE, 2-time 2-plane correlations reveal that high/low reference-plane-averaged TKE precedes high/low plane-averaged TPR in both the core and near-wall regions when taking the reference plane in the outer near-equilibrium region. In this reference plane, plane-averaged TKE and plane-averaged TPR are anti-correlated with positive time lag from high/low TKE to low/high TPR.

We have explained these TPR observations with a mechanistic model. High instantaneous Reynolds shear stress flattens the local mean flow profile (reduces the local mean shear) in the near-equilibrium region as ejections and sweeps mix high streamwise momentum above with low streamwise momentum below the reference plane. It then strengthens the mean shear in the near-wall region as high streamwise momentum is brought close to the wall, where viscosity kicks in.

Acknowledgements. This work is granted access to the HPC resources of IDRIS under the allocation 2022-021741 made by GENCI (Grand Equipement National de Calcul Intensif).

Funding. This work is supported by the European Office of Aerospace Research and Development (EOARD) (FA8655-21-1-7016, program manager Dr D. Smith).

Declaration of interests. The authors report no conflict of interest.

Author ORCIDs.
Le Yin https://orcid.org/0009-0008-3635-7841;
Yongyun Hwang https://orcid.org/0000-0001-8814-0822;
John Christos Vassilicos https://orcid.org/0000-0003-1828-6628.

References

Apostolidis, A., Laval, J.-P. & Vassilicos, J.C. 2022 Scalings of turbulence dissipation in space and time for turbulent channel flow. *J. Fluid Mech.* **946**, A41.

Bewley, T. 2014 *Numerical Renaissance: Simulation, Optimization, and Control*. Renaissance Press.

Cheng, C., Shyy, W. & Fu, L. 2022 Streamwise inclination angle of wall-attached eddies in turbulent channel flows. *J. Fluid Mech.* **946**, A49.

Ciola, N., De Palma, P., Robinet, J.-C. & Cherubini, S. 2023 Nonlinear optimal perturbation of turbulent channel flow as a precursor of extreme events. *J. Fluid Mech.* **970**, A6.

Doohan, P., Bengana, Y., Yang, Q., Willis, A.P. & Hwang, Y. 2022 The state space and travelling-wave solutions in two-scale wall-bounded turbulence. *J. Fluid Mech.* **947**, A41.

Doohan, P., Willis, A.P. & Hwang, Y. 2019 Shear stress-driven flow: the state space of near-wall turbulence as $Re_\tau \to \infty$. *J. Fluid Mech.* **874**, 606–638.

Doohan, P., Willis, A.P. & Hwang, Y. 2021 Minimal multi-scale dynamics of near-wall turbulence. *J. Fluid Mech.* **913**, A8.

Farano, M., Cherubini, S., Robinet, J.-C. & De Palma, P. 2017 Optimal bursts in turbulent channel flow. *J. Fluid Mech.* **817**, 35–60.

Flores, O. & Jiménez, J. 2010 Hierarchy of minimal flow units in the logarithmic layer. *Phys. Fluids* **22** (7), 071704.

Frisch, U. 1995 *Turbulence: The Legacy of A.N. Kolmogorov*. Cambridge University Press.

Goto, S. & Vassilicos, J.C. 2015 Energy dissipation and flux laws for unsteady turbulence. *Phys. Lett.* A **379** (16), 1144–1148.

Goto, S. & Vassilicos, J.C. 2016 Local equilibrium hypothesis and Taylor's dissipation law. *Fluid Dyn. Res.* **48** (2), 021402.

Guala, M., Hommema, S.E. & Adrian, R.J. 2006 Large-scale and very-large-scale motions in turbulent pipe flow. *J. Fluid Mech.* **554**, 521–542.

HAMILTON, J.M., KIM, J. & WALEFFE, F. 1995 Regeneration mechanisms of near-wall turbulence structures. *J. Fluid Mech.* **287**, 317–348.
HOYAS, S. & JIMÉNEZ, J. 2006 Scaling of the velocity fluctuations in turbulent channels up to $Re_\tau = 2003$. *Phys. Fluids* **18** (1), 011702.
HUTCHINS, N. & MARUSIC, I. 2007*a* Evidence of very long meandering features in the logarithmic region of turbulent boundary layers. *J. Fluid Mech.* **579**, 1–28.
HUTCHINS, N. & MARUSIC, I. 2007*b* Large-scale influences in near-wall turbulence. *Phil. Trans. R. Soc. Lond.* A **365** (1852), 647–664.
HWANG, Y. & BENGANA, Y. 2016 Self-sustaining process of minimal attached eddies in turbulent channel flow. *J. Fluid Mech.* **795**, 708–738.
HWANG, Y. & COSSU, C. 2010 Self-sustained process at large scales in turbulent channel flow. *Phys. Rev. Lett.* **105**, 044505.
JIMÉNEZ, J. & MOIN, P. 1991 The minimal flow unit in near-wall turbulence. *J. Fluid Mech.* **225**, 213–240.
JIMÉNEZ, J. & PINELLI, A. 1999 The autonomous cycle of near-wall turbulence. *J. Fluid Mech.* **389**, 335–359.
KIM, J. & MOIN, P. 1985 Application of a fractional-step method to incompressible Navier–Stokes equations. *J. Comput. Phys.* **59** (2), 308–323.
KIM, K.C. & ADRIAN, R.J. 1999 Very large-scale motion in the outer layer. *Phys. Fluids* **11** (2), 417–422.
KLINE, S.J., REYNOLDS, W.C., SCHRAUB, F.A. & RUNSTADLER, P.W. 1967 The structure of turbulent boundary layers. *J. Fluid Mech.* **30** (4), 741–773.
KWON, Y.S., PHILIP, J., DE SILVA, C.M., HUTCHINS, N. & MONTY, J.P. 2014 The quiescent core of turbulent channel flow. *J. Fluid Mech.* **751**, 228–254.
LEE, M. & MOSER, R.D. 2015 Direct numerical simulation of turbulent channel flow up to $Re_\tau \approx 5200$. *J. Fluid Mech.* **774**, 395–415.
LOZANO-DURÁN, A. & JIMÉNEZ, J. 2014*a* Effect of the computational domain on direct simulations of turbulent channels up to $Re_\tau = 4200$. *Phys. Fluids* **26** (1), 011702.
LOZANO-DURÁN, A. & JIMÉNEZ, J. 2014*b* Time-resolved evolution of coherent structures in turbulent channels: characterization of eddies and cascades. *J. Fluid Mech.* **759**, 432–471.
LU, S.S. & WILLMARTH, W.W. 1973 Measurements of the structure of the Reynolds stress in a turbulent boundary layer. *J. Fluid Mech.* **60** (3), 481–511.
MARUSIC, I. & HEUER, W.D.C. 2007 Reynolds number invariance of the structure inclination angle in wall turbulence. *Phys. Rev. Lett.* **99**, 114504.
PIROZZOLI, S. 2023 Searching for the log law in open channel flow. *J. Fluid Mech.* **971**, A15.
SAGAUT, P. & CAMBON, C. 2008 *Homogeneous Turbulence Dynamics*. Cambridge University Press.
TOWNSEND, A.A. 1961 Equilibrium layers and wall turbulence. *J. Fluid Mech.* **11** (1), 97–120.
VASSILICOS, J.C. 2015 Dissipation in turbulent flows. *Annu. Rev. Fluid Mech.* **47** (1), 95–114.
VASSILICOS, J.C. & LAVAL, J.-P. 2024 Scale-by-scale non-equilibrium in turbulent flows. In *Coarse Graining Turbulence: Modeling and Data-Driven Approaches and their Applications* (ed. F.F. Grinstein, F.S. Pereira & M. Germano). Cambridge University Press.
WALEFFE, F. 1997 On a self-sustaining process in shear flows. *Phys. Fluids* **9** (4), 883–900.
WALLACE, J.M., ECKELMANN, H. & BRODKEY, R.S. 1972 The wall region in turbulent shear flow. *J. Fluid Mech.* **54** (1), 39–48.
WILLMARTH, W.W. & LU, S.S. 1972 Structure of the Reynolds stress near the wall. *J. Fluid Mech.* **55** (1), 65–92.
YAO, J., CHEN, X. & HUSSAIN, F. 2022 Direct numerical simulation of turbulent open channel flows at moderately high Reynolds numbers. *J. Fluid Mech.* **953**, A19.